#51
QUARTERLY
Newsletter

Special issue

Mercator Ocean
Ocean Forecasters

ICE-ARC
ICE • CLIMATE • ECONOMICS

6th International Workshop on Sea-Ice Modelling and Data Assimilation
2014 Sept 15-16, Toulouse, France

The EU FP7 ICE-ARC Project and the International Ice Charting Working Group (IICWG) held a workshop on Sea-Ice Modelling and Data Assimilation in Toulouse (France) on September 15-16 2014. It was also a key-event for the MyOcean2 project. The two-day workshop was hosted by Mercator Ocean, one of the ICE-ARC partners, and 38 people from 9 countries all over Europe and Canada attended.

Credits: Mercator-Ocean

Editorial – March 2015 – Special Issue jointly coordinated by Mercator Ocean with ICE-ARC and IICWG focusing on Sea Ice Modelling and Data Assimilation.

Greetings all,

For the first time, the Mercator Ocean Forecasting Center in Toulouse and the ICE-ARC as well as IICWG projects publish together a special issue of the newsletter dedicated to sea ice modelling and data assimilation.

The EU FP7 ICE-ARC Project and the International Ice Charting Working Group (IICWG) held a workshop on Sea-Ice Modelling and Data Assimilation in Toulouse (France) on September 15-16 2014. It was also a key-event for the MyOcean2 project. This special issue reports on a representative selection of works presented at this workshop. The two-day workshop was hosted by Mercator Ocean, one of the ICE-ARC partners, and 38 people from 9 countries all over Europe and Canada attended. The focus was put on research and development related to numerical sea ice analysis and prediction. General topics included:

- Sea ice observations and uncertainties
- Sea ice data assimilation (methods and results)
- Sea ice model parameterizations and coupling to ocean and atmosphere models
- Verification approaches for sea-ice analyses and forecasts

The four first papers present the ICE-ARC, ACCESS, PPP/YOPP and IAOOS projects.

- ICE-ARC (Ice, Climate, Economics – Arctic Research on Change) is a four year (2014-2018) EU-funded project which brings together physicists, chemists, biologists, economists, and sociologists from 21 institutes from 11 countries across Europe. With a budget of €11.5M, it aims at understanding and quantifying the multiple stresses involved in the change in the Arctic marine environment.
- ACCESS is a European Project (2011-2015) supported by the Ocean of Tomorrow call of the European Commission Seventh Framework Programme. Its main objective is to assess climatic change impacts on marine transportation (including tourism), fisheries, marine mammals and the extraction of oil and gas in the Arctic Ocean. ACCESS is also focusing on Arctic governance and strategic policy options.
- One of the key elements of the WWRP (WORLD WEATHER RESEARCH PROGRAMME from the WORLD METEOROLOGICAL ORGANIZATION, i.e. WMO) Polar Prediction Project is The Year of Polar Prediction (YOPP) which will consider both the Arctic and Antarctic, and is scheduled to take place from mid 2017 to mid 2019. The intention is to have an extended period of coordinated intensive observational and modelling activities in order to improve polar prediction capabilities on a wide range of time scales. YOPP is a contribution to the hourly to seasonal research component of the WMO Global Integrated Polar Prediction System (GIPPS).

- IAOOS (Ice Atmosphere Ocean Observing System, http://www.iaoos-equipex.upmc.fr, http://iaoos.ipev.fr/) is a nine-year French-funded project (2011-2019), developed by LOCEAN and LATMOS, which objective is to provide and maintain an integrated observing system over the Arctic Ocean that collects synoptic and near real time information related to the state of the atmosphere, the snow, the sea-ice and the ocean. The IAOOS system involves 15 autonomous platforms operating at any given time in the Arctic Ocean for a total period of 5 years (2015-2019) and collecting synoptic and near real time information related to the state of the lower atmosphere, the sea-ice and the upper ocean.

Then, aspects about operational sea ice forecasting are displayed in the three next papers by Peterson, Buehner et al. and finally in Garric et al. :

- Peterson presents the UK Metoffice GloSea5 Coupled Seasonal Forecast System which has sea ice fields initialized with the FOAM ocean and sea ice system with assimilation of SSM/I satellite sea ice concentration observations along with ocean surface and sub-surface observations. He presents the seasonal forecast of September sea ice extent emphasizing the problems associated with too thin initial ice thickness conditions.
- Then Buehner et al. display the progress in sea ice data assimilation at Environment Canada. They describe the current configuration of the analysis component of the Environment Canada Regional Ice Prediction System and recent research results from the assimilation of high resolution visible/infrared satellite data.
- Finally, Garric et al. describe the recent developments impacting the sea ice in the Mercator Océan French Operational Oceanography Center global ¼° configuration. Two main developments in the NEMO-based model component are tested: (i) the multi-category LIM3 sea ice model and (ii) the comprehensive representation of the freshwater flux from polar ice sheets.

The two last papers by Lupkes et al. and Dansereau et al. display specific parameterization aspects:

- Lupkes et al. describe a new parameterization of drag coefficients accounting for the impact of edges at ice floes, leads, and melt ponds on momentum transport. The parameterization is evaluated for idealized meteorological forcing in the Siberian and Central Arctic. The distributions of drag coefficients obtained from traditional parameterizations and from the new one show large differences in their test scenario especially in the region south of 80°N.
- Dansereau et al. present a new dynamical model built on the elasto-brittle (EB) rheology and which is developed in the context of the operational modeling of sea ice conditions over the Arctic. The EB model is modified and tested in early idealized simulations. Results show that the model is able to reproduce the strong heterogeneity and intermittency and the anisotropy that characterize the deformation of sea ice.

We wish you a pleasant reading,

Laurence Crosnier and Gilles Garric, Editors.

Contents:

ICE ARC Project

By J. Wilkinson [1]

[1] *British Antarctic Survey, Cambridge, UK*

Arctic change impacts the local, regional and global climate through complex coupling mechanisms within the Earth system. However these are not the only changes the Arctic is going through. It is predicted that commercial investment in the Arctic could reach $100bn or more in the coming decade, with oil and gas, mining and the shipping industries being the biggest drivers. The environmental, socio-economic and geopolitical consequences of Arctic change will be considerable.

Because of the seriousness of this situation we have to ensure that national and international politicians and policy-makers, as well as industry and the public, have the most up-to-date and robust science available on Arctic change. Evidence based and not ideological based decision-making is fundamental to ensure that informed policy decisions can be reached.

With these substantial issues in mind our EU funded programme ICE-ARC (http://www.ice-arc.eu/) (Ice, Climate and Economics:- Arctic Research on Change) assess the climatic (sea ice, ocean, atmosphere and ecosystem), economic and social impacts of these stresses on both a regional and global scale.

Our joined up approach enables the results from our basin wide observational programme to be used directly by our modelling programme. The resulting projections of theses models will be fed into an economic impact assessment model that will calculate the monetary value associated with the projected physical changes upon the global economic and social system. This will be the first time the impact of Arctic change, observed and projected, has on the global economy. The outputs of the ICE-ARC will undoubtedly lead to more effective policy and management options for societal responses to climate change.

ICE-ARC objectives include:

- Improved climate prediction for the Arctic Ocean and the reduction of uncertainties in those predictions;
- Improved understanding of climate change impacts on marine ecosystems;
- Assessment of socio-economic vulnerabilities, both to the peoples of the north and to the planet as a whole;
- Improved National, European and International Arctic marine policies to cope with the implications of an increasingly ice-free Arctic;
- Improved understanding of the living resources for Arctic human communities;
- Effective policy and management options for societal responses to climate change.

ICE-ARC brings together leading experts from 21 Institutions in 11 European countries. Of these countries three border the Arctic Ocean (Greenland/ Denmark, Norway and Russia) and are permanent members of the Arctic Council

ASSESSING CLIMATE CHANGE IMPACTS ON MARINE ECOSYSTEMS AND HUMAN ACTIVITIES IN THE ARCTIC OCEAN: THE EUROPEAN ACCESS PROGRAMME (2011-2015)[1]

By Jean-Claude Gascard (coordinator)[1], Michael Kärcher (co-coordinator)[2], Mélanie Pellen (project manager)[3], Nathalie Sennechael (communication leader)[3] and Thomas Bonnin (communication assistant)[3].

Have also provided their help in reviewing this article:
Christine Provost (IAOOS project co-coordinator)[3]
Michael Field (engineer)[3]

[1] LOCEAN, UPMC and CNRS, France.
[2] OASYS, Germany
[3] LOCEAN, UPMC, France

1- ORIGINS OF ACCESS

Supported by the Ocean of Tomorrow call of the European Commission Seventh Framework Program, the four-year ACCESS program began in 2011, building on the legacy of a major European Union (EU) program, DAMOCLESi (2005-2010), devoted to the development of environmental observation and modelling systems of the Arctic Ocean. Coordinated by the LOCEANii laboratory at the University Pierre et Marie Curie, Paris, France, ACCESS involves more than 80 researchers from 9 European countries and the Russian Federation (the complete list of the ACCESS consortium members is included after the article's references).

Figure 1: Danish company Nordic Bulk Carriers A/S's vessel "Nordic Orion" using for the first time ever the North West Passage in September 2013 between Vancouver and the port of Pori in Finland.

2- ACCESS CONTEXT AND OBJECTIVES

As can be observed in the reduction of sea-ice (figure1), changes in weather patterns and cyclones or in the melting of glaciers and permafrost, the Arctic is engaged in a significant climatic evolution. This evolution is quite predictable at long time scales (several decades), but the short (decadal and intermediate) scale is the most difficult to predict. This can be explained by the natural variability of the system which is large and dominant at this short scale, and the high non-linearity of the system due to positive and negative feedback between sea ice, ocean and atmosphere. Models predict that Artic sea ice will disappear in summer within 20 or 30 years, yielding new opportunities and risks for human activities in the Arctic, which in turn have important socio-economic implications for Europe.
While former Arctic programs were primarily dedicated to physical sciences, ACCESS (figure 2) developed an interdisciplinary approach with the main objective to assess long-term climate change impacts on marine transportation (including tourism), fisheries, marine mammals and the extraction of oil and gas in the Arctic Ocean.iii Quantification of these impacts on economic sectors and the evaluation of associated risks require a precise knowledge of the state of the Arctic climate system. As such, studying the future evolution of Arctic sea-ice, atmosphere and ocean is one of the major

Assessing climate change impacts on marine ecosystems and human activities in the Arctic ocean: the european ACCESS programme (2011-2015)[1]

ACCESS overarching activities. ACCESS is also conducting a challenging cross-sectorial integrated program dedicated to governance options that can be considered by decision makers to ensure sustainable development and environmental protection of the Arctic Ocean.
Recognizing the difficulty for current climate models and scenarios to reproduce recent changes in the Arctic environment, an important objective of ACCESS is to improve scenarios for environmental changes that could result from increased economic activity in the Arctic for the next three decades.

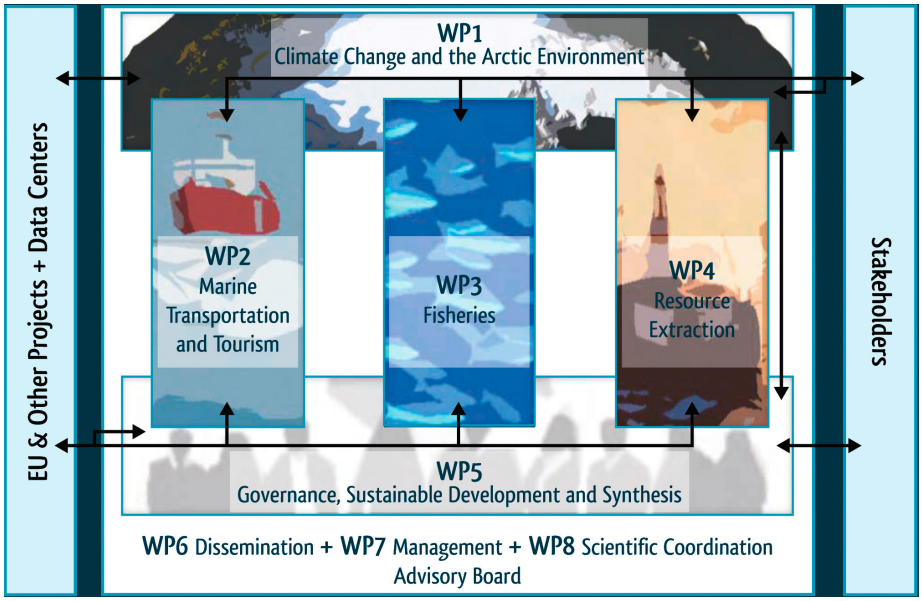

Figure 2: ACCESS Work Packages.

Since the autumn of 2014, the ACCESS team started finalizing and summarizing its results. The project's last General Assembly is scheduled for 24-26 February in Villanova (Spain) and the program will end on 28 February 2015. Continuing in its footsteps, the British Antarctic Survey-coordinates the ICE-ARCiv, project launched on 1 January 2014 with the aim to evaluate the social and economic impact of Arctic sea-ice loss.

3- ACCESS DISSEMINATION AND OUTREACH

The broad remit of ACCESS research makes the project's outputs relevant to different groups of stakeholders, including policy makers, the industrial and academic sectors and the larger public.
The ACCESS dissemination and exploitation plan is organized around a double perspective:

1) « dissemination and public outreach » will make available the results of the project,
2) « exploitation of knowledge » will gather all existing data in the different project domains in order to make them available via databases or portals.

A list of the project's deliverables can be found online.

Figure 3: ACCESS scientists and graduate students at the 2nd ACCESS Summer School in Stockholm, 2014. Photo: courtesy of Aliaksei Patonia.

Important dissemination events for ACCESS, two cross-sectorial summer schools (figure 3) were organized with the aim of providing students with an opportunity to learn and interact with ACCESS experts about different aspects of Arctic resilience and changes in the region's economic sectors. Students were also provided with the opportunity to present their results to the experts and publish them in the ACCESS Newsletter.
The Bremen summer school (September 2013) notably facilitated the young scientists to develop their own ideas on cross-sectorial subjects such as how researchers can better interact with indigenous populations. The Stockholm session (September 2014) concentrated on specific economic sectors and their interactions in the context of climate change in the Arctic Ocean as well as ongoing efforts to develop syntheses and systemic overviews using tools like marine spatial planning and resilience assessments. Participants also worked to interpret and discuss selected social-ecological cases studies as specific examples of changing Arctic conditions, linking the climate, ecologic, economic and other social dimensions.
Another key outreach action for ACCESS was the meeting with representatives of indigenous groups of the Arctic Council held in Paris on July 9 and 10 2014. The aim was to understand how the results of the ACCESS project can better help the Indigenous People of the Arctic and to ensure, as far as possible, that different Indigenous People views are appropriately integrated with relevant ACCESS tasks and deliverables. The event was co-organized with the ICE-ARC program.

4- SELECTION OF ACCESS HIGHLIGHTED RESULTS

Here follows an overview of selected works achieved during ACCESS, mainly based on the project's eleven newsletters (referred to as NL hereafter).

WORKPACKAGE 1 CLIMATE CHANGE IN THE ARCTIC

- Research synthesis and predictions of Arctic climate variability for the next 30 years was the focus of a workshop held at Villefranche Oceanographic Laboratory in June 2014. (NL9)
- Sea-ice extent observations based on satellite AMSR-E observations showing the advance of the melt onset and sea-ice break up during early Spring as well as the freeze up delayed during late Fall over the past 10 years. (NL3)
- Sea-ice observations in the Chukchi Sea (2011) comparing temporal variation of cumulative solar input versus the heat required for the observed melting rate along ice floes trajectories. (NL3)
- Oceanographic observations obtained during the past 10 years in the northern Laptev Sea showing the increasing temperature of the Atlantic core penetrating into the Arctic Ocean. (NL3)
- From July and October 2013, circumnavigation of the French schooner Tara for ACCESS fieldwork activity. (NL5)
- The deployment of an ACOBAR Ice drift station at the North Pole in April 2012 revealed the presence of a surface salinity front at about 87°N separating the Arctic Ocean in two distinct regions influenced by the North Atlantic Ocean on one side and by the North Pacific Ocean on the other side. (NL5)
- The deployment (2012) of ACCESS and KOPRI sea ice mass balance buoys allowed to measure differential melt and growth rates at different ice types under the same oceanic and atmospheric forcings. (NL5)
- Documention and analysis of changing conditions in the upper water layer in the Atlantic sector of the Arctic Ocean in connection with decreasing sea-ice cover. (NL6)
- Calculation of freezing and melting degrees day anomalies in the Arctic Ocean over three decades. (NL6)
- First mission of a glider in the Barents Sea demonstrating the monitoring potential of such equipment. (NL11)
- Applications from the Earth system Model (ESM) showing the effect of increasing resolution for precipitation over the Nordic Seas, Scandinavia and the Barents Sea.
- Applications from the AWI model (NAOSIM) investigating short time forecasting capabilities for sea-ice concentration pointing the essential role of initial sea-ice thickness distributions.
- Modelling impacts of local sources of air pollution from shipping and oil/gas extraction on atmospheric composition. (NL4)

WORKPACKAGE 2 TRANSPORT AND TOURISM

- Assessment of current monitoring and forecasting requirements from users and international providers. (NL3)
- Estimation of the effects of climate change on tourism in the Arctic based on an extension of the Hamburg Tourism Model (HTM), a climate change tourism simulation model. (NL6)
- Analysis of historical sea-ice data and their influence on navigation along the Northern Sea Route (NSR) in the 20th and early 21st centuries. (NL6)
- Estimation of navigation efficiency along the NSR under past climate situations in comparison with various climate change scenarios and recommendations for navigation based on present sea-ice conditions along the NSR and other navigational routes in the Arctic. (NL6)
- Calculation of fuel consumption and emissions for various ship types in ice-covered waters (NL11). The brief paper n°2 explores links between Arctic shipping, air pollution and climate change. It recaps why it matters and some policy approaches adopted or under consideration to tackle the issues. ACCESS Policy Brief n°2: « Shipping in the Arctic: Links to Air Pollution and Climate Change ».

WORKPACKAGE 3 FISHERIES

- Identification of governance gaps within the existing frameworks regulating activities in the Arctic Ocean: the lack of regional fisheries management systems for the Arctic Ocean, the absence of any provisions in place in the developing IMO Polar Code with respect to climate change effects and a fragmented approach to regulations for the resource exploitation industry. (NL3)
- Investigation of the current state of coastal communities (including indigenous populations) in the Barents region under the changing environmental, economic and political conditions. (NL5)
- Phyto- and zoo-plankton productivity modeling underlying the fisheries industry in the Barents Sea until the end of this century (NL3, NL6). Arctic fishing and aquaculture enterprises are an important source of seafood for the European Union (EU) and global markets. The brief paper n°3 explores how this could be impacted with climate change. ACCESS Policy Brief n°3: « Seafood production in a changing Arctic ».

WORKPACKAGE 4 RESOURCE EXTRACTION

- Development of an under ice oil trajectory model to allow accurate appraisal of oil movement under sea ice along with the potential oil holding capacity of sea ice. (NL2)
- Experiments in a controllable tank provided a better understanding and parameterization of oil spill in ice covered seas. (NL3)
- Review of existing technologies for offshore production of hydrocarbons and identification of gaps preventing adoption of existing hydrocarbons exploitation technologies under Arctic conditions. (NL3)
- Research on risks and impacts of shipping and resources extraction in Arctic waters. (NL8, NL11)
- Escape, Evacuation and Rescue from Arctic Facilities. (NL6)
- Analysis of the social and economic impacts of hydrocarbons production in the Arctic region. (NL3, NL11)
- Test flights of the concentration of hydrocarbons, sulfur dioxide, volatile aerosols in the plumes of oil and gas platform emissions and other parameters clearly detected in the vicinity of oil & gas extraction facilities. (NL3)
- Observation, modeling and management of the impacts of underwater noise on marine mammals from shipping and seismic operations in the Arctic. (NL3, NL8)
- The brief paper n°1 explores the impact and consequences of an oil spill in the Arctic marine environment ACCESS Policy brief n°1: « Oil spill response capabilities and technologies in ice-covered waters ».

WORKPACKAGE 5 ARCTIC GOVERNANCE, SUSTAINABLE DEVELOPMENT AND SYNTHESIS.

- Use of the Marine Spatial Planning to conduct an integrated ocean management assessment where strategic options for promoting the conservation and sustainable use of the marine environment can be developed. (NL2, NL7)
- Analysis and synthesis of existent and developing regulatory frameworks. (NL3)
- Interdisciplinary modelling activities to be better able to project a range of potential future states of Arctic sea-ice distribution and variability. Such future scenarios are necessary to illustrate strategies to estimate and interpret the impacts of climate change and identify infrastructure and policy options for addressing the socio-economic impacts of activities in the Arctic Ocean. (NL4)
- Cross-sectorial synthesis meetings and ACCESS summer school in Bremen (NL6) and Stockholm. (NL11)
- Workshop in Paris with representatives of Indigenous Peoples organizations of the Arctic Council. (NL10)

References

[1] ACCESS (Arctic Climate Change, Economy and Society, 2011-2015): www.access-eu.org
[2] DAMOCLES (Developing Arctic Modeling and Observing Capabilities for Long-term Environmental Studies): http://www.damocles-eu.org
[3] LOCEAN (Laboratoire d'Océanographie et du Climat : Expérimentations et Approches Numériques): https://www.locean-ipsl.upmc.fr University Pierre et Marie Curie (UPMC), Paris: http://www.upmc.fr
[4] ACCESS objectives and workpackages are detailed on the project's website: www.access-eu.org
[5] ICE-ARC (Ice, Climate, Economics - Arctic Research on Change): http://www.ice-arc.eu/

No	Name	Short name	Country	No	Name	Short name	Country
1	UNIVERSITE PIERRE ET MARIE CURIE - PARIS 6	UPMC	France	15	P.P. SHIRSHOV INSTITUTE OF OCEANOLOGY OF RUSSIAN ACADEMY OF SCIENCES	SIO	Russian Federation
2	O.A. SYS - OCEAN ATMOSPHERE SYSTEMS GMBH	Oasys	Germany	16	IMPAC OFFSHORE ENGINEERING GMBH	IMPaC	Germany
3	NATURAL ENVIRONMENT RESEARCH COUNCIL	NERC	United Kingdom	17	UNIVERSITAT POLITECNICA DE CATALUNYA	UPC	Spain
4	INSTITUT FUR WELTWIRTSCHAFT	Kiel IfW	Germany	18	DEUTSCHES ZENTRUM FUER LUFT - UND RAUMFAHRT EV	DLR	Germany
5	THE CHANCELLOR, MASTERS AND SCHOLARS OF THE UNIVERSITY OF CAMBRIDGE	UCAM	United Kingdom	19	ARCTIC AND ANTARCTIC RESEARCH INSTITUTE	AARI	Russian Federation
6	ALFRED-WEGENER-INSTITUT FUER POLAR- UND MEERESFORSCHUNG	AWI	Germany	20	ECONOMIC AND SOCIAL RESEARCH INSTITUTE	ESRI	Ireland
7	SCHWARZ JOACHIM REINHOLD FRANZ	JSC	Germany	21	LAPIN YLIOPISTO	UoL	Finland
8	NOFIMA MARIN AS	NOFIMA	Norway	22	SINTEF FISKERI OG HAVBRUK AS	SINTEF F&H	Norway
9	HAMBURGISCHE SCHIFFBAU-VERSUCHSANSTALT GMBH	HSVA	Germany	23	CICERO SENTER KLIMAFORSKNING STIFTELSE	CICERO	Norway
10	NORSK POLARINSTITUTT	NPI	Norway	24	STIFTELSEN SINTEF	SINTEF	Norway
11	METEOROLOGISK INSTITUTT	Met.no	Norway	25	GESELLSCHAFT ZUR FORDERUNG DES ENERGIEWIRTSCHAFTLICHEN INSTITUTS AN DER UNIVERSITAT ZU KOLN GGMBH - EWI	EWI	Germany
12	FASTOPT GMBH	FastOpt	Germany	26	LE CERCLE POLAIRE ASSOCIATION	LCP	France
13	THE SCOTTISH ASSOCIATION FOR MARINE SCIENCE	SAMS	United Kingdom	27	NORDIC BULK CARRIERS AS	NBC	Denmark
14	KUNGLIGA VETENSKAPSAKADEMIEN	Beijer Institute	Sweden				

Figure 4: ACCESS consortium members.

The Year of Polar Prediction (YOPP): Challenges and Opportunities in Ice-Ocean Forecasting

By G. C. Smith[1], T. Jung[2], N. D. Gordon[3], S. Klebe[2], H. Goessling[2], P. Bauer[4], D. Bromwich[5], M. Chevallier[6], J. Day[7], F. Doblas-Reyes[8], M. Holland[9], J. Inoue[10], T. Iversen[11], Peter Lemke[2], A.P. Makshtas[12], Brian Mills[13], P. Nurmi[14], I. Renfrew[15], P. Reid[16], G. Svensson[17], M. Tolstykh[18], Q. Yang[19]

[1] Environment Canada, Meteorological Research Division, Dorval, Canada
[2] Alfred Wegener Institute, Helmholtz Centre for Polar and Marine Research, Bremerhaven, Germany
[3] Neil Gordon, New Zealand
[4] European Centre for Medium-Range Weather Forecasts, Model Division Research Department, Shinfield Park, Reading, UK
[5] Polar Meteorology Group, Byrd Polar Research Center, Ohio State University, Columbus, Ohio, USA
[6] Meteo-France, Toulouse, France
[7] University of Reading,Dept. of Meteorology, Reading, UK
[8] ICREA, Institut Català de Ciències del Clima, Barcelona, Spain
[9] National Center for Atmospheric Research, Climate and Global Dynamics Division, Boulder, Colorado, USA
[10] National Institute of Polar Research , Tokyo, Japan
[11] Norwegian Meteorological Institute, Present Affiliation: European Centre for Medium-Range Weather Forecasts, Shinfield Park, Reading, United Kingdom
[12] Arctic and Antarctic Research Institute, St. Petersburg, Russian Federation
[13] Meteorological Research Division, Environment Canada, c/o Faculty of Environment, University of Waterloo, Waterloo, ON
[14] Finnish Meteorological Institute R&D, Meteorological Research, Helsinki, Finland
[15] School of Environmental Sciences, University of East Anglia, Norwich Research Park, Norwich, United Kingdom
[16] Bureau of Meteorology, Hobart, Australia
[17] Department of Meteorology and Bert Bolin Centre for Climate research, Stockholm University, Stockholm, Sweden
[18] Hydrometcentre of Russia, Moscow, Russian Federation
[19] Polar Environmental Research and Forecasting Division, National Marine Environmental Forecasting Center, Beijing, China

Introduction

In response to a growing interest in the Arctic in recent years, the number of real-time short-medium range sea ice prediction systems has been increasing, and now includes several systems covering the full Arctic Ocean, for example: the Arctic Cap Nowcast/Forecast System (ACNFS; Posey et al., 2010), Towards an Operational Prediction system for the North Atlantic European coastal Zones (TOPAZ; Bertino and Lisæter, 2008), and the Canadian Centre for Marine and Environmental Prediction's Global Ice Ocean Prediction System (GIOPS; Smith et al., 2015) and Regional Ice Prediction System (RIPS; Lemieux et al., 2015; Buehner et al., 2013). In addition, numerous ice-ocean hindcasts[1] and reanalyses have been made and intercompared through the Arctic Ocean Model Intercomparison Project (AOMIP; Johnson et al., 2007) and the CLIVAR Global Synthesis and Observations Panel (GSOP) Ocean Reanalysis Intercomparison Project (ORA-IP; Balmaseda et al., 2015). Despite this significant effort, it is difficult to ascertain the true skill of these prediction systems and their primary sources of error, as reliable observations are limited and verification techniques tend to vary from one group to another. As a result, the potential benefits of sea ice prediction for various user groups (e.g. national ice services, marine transportation and resource exploitation, coupling with numerical weather prediction) have been hindered by uncertainty regarding the skillfulness of predictions and how best to use them. An intercomparison of sea ice fields from existing systems by the GODAE Oceanview Intercomparison and Validation Task Team (www.godae.org) has been initiated, although a larger coordinated international effort is needed. The upcoming Year of Polar Prediction (YOPP) aims to address these challenges in the context of a broader initiative toward improved polar environmental predictions for both hemispheres.

[1] *Here we use the term 'hindcast' to refer to free running continuous simulations with no data assimilation*

The Year of Polar Prediction

YOPP is a period of intensive observing, modelling, verification, user-engagement and education activities (Fig. 1) planned for mid-2017 to mid-2019, centred on 2018. Its goal is to enable a significant improvement in environmental prediction capabilities for the Polar Regions and beyond, including ice-ocean forecasting.

YOPP is a major initiative of WMO's World Weather Research Programme Polar Prediction Project (WWRP-PPP), and is being planned and coordinated by a Planning Group comprising the PPP Steering Group together with representatives from partners and other initiatives, including the World Climate Research Programme's (WCRP) Polar Climate Predictability Initiative (PCPI).

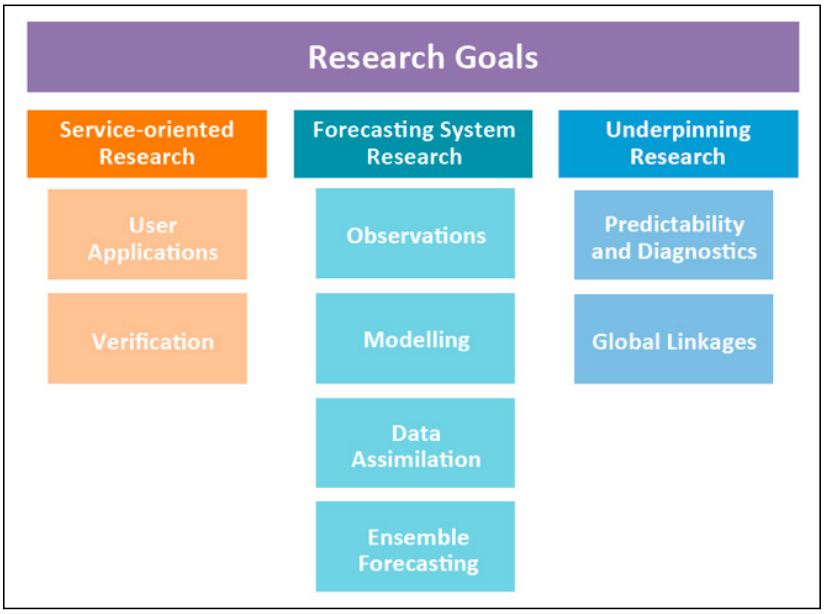

Fig. 1: Research Goals for the Year of Polar Prediction

The objectives of YOPP are to:

1. Improve the polar observing system to provide better coverage of high-quality observations in a cost effective manner.
2. Gather additional observations through field programmes aimed at improving understanding of key polar processes.
3. Develop improved representation of key polar processes in uncoupled and coupled models used for prediction, including those which are particular hindrances to high-quality prediction for the Polar Regions, such as those relating to stable boundary layer representation, surface exchange, permafrost, mixed phase clouds, winds, extreme thermal contrasts, and steep orography.
4. Develop improved data assimilation systems that account for challenges in the Polar Regions such as sparseness of observational data, steep orography, cryosphere uncertainties, model error and the importance of coupled processes (e.g., atmosphere-sea ice interaction).
5. Explore the predictability of the atmosphere-cryosphere-ocean, with a focus on sea ice, on time scales from days to a season.
6. Improve understanding of linkages between Polar Regions and lower latitudes and assess skill of models representing these.
7. Improve verification of polar weather and environmental predictions to obtain quantitative knowledge on model performance and on the skill of operational forecasting systems for user-relevant parameters; and efficiently monitor progress.
8. Improve understanding of the benefits of using existing prediction information and services in the Polar Regions, differentiated across the spectrum of user types and benefit areas.
9. Provide training opportunities to generate a sound knowledge base on polar prediction related issues.

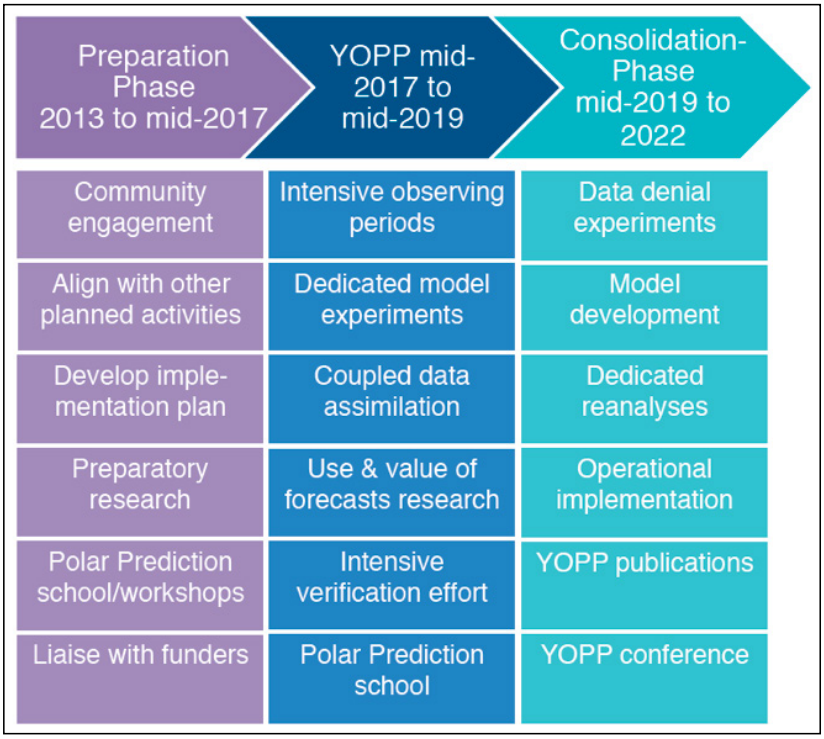

During the YOPP Preparation Phase (until mid-2017; Fig. 2) plans will be further developed through international workshops, there will be engagement with stakeholders and arrangement of funding, coordination of observations and models, and preparatory research. YOPP from mid-2017 to mid-2019 encompasses four major elements: an intensive observing period, a complementary intensive modelling and forecasting period, a period of enhanced monitoring of forecast use in decision making including verification, and a special educational effort. The YOPP Consolidation Phase from mid-2019 to 2022 will provide a legacy of data and publications, as well as implementation of YOPP findings to achieve the significant improvement in environmental prediction capabilities for the Polar Regions - and beyond, through linkages with lower latitudes.

Fig. 2:
Overview of the three phases of the Year of Polar Prediction

Main Elements of YOPP

An important aspect of YOPP will be the coordination of field experiments. A particularly interesting field experiment, currently being planned, is the Multidisciplinary drifting Observatory for the Study of Arctic Climate (MOSAiC; www.mosaicobservatory.org). MOSAiC will be based around a polar research vessel starting in newly formed Arctic sea ice around September 2018, and drifting with the ice over the course of at least a year, to study a full annual cycle. The project is specifically designed to study interdisciplinary process interactions linking the central Arctic sea-ice, atmosphere, ocean, and biosphere. There will also be a number of Intensive Observing Periods. A re-initiation of the Russian drifting platform is also planned for YOPP, which would provide highly complementary observations to MOSAiC.

Satellites provide unique observational capabilities for the atmosphere, oceans and cryosphere. It will be crucial to exploit the available satellite data during YOPP. Providing researchers and stakeholders with comprehensive satellite-based sea ice products will be crucial to advance sea ice data assimilation and prediction capabilities in the coming years. In particular, providing reliable near real-time information about ice thickness and deformation characteristics of sea ice (leads and pressure ridges) will be key.

YOPP will also take advantage of the existing operational data gathered over Polar Regions, and will promote the augmentation of current monitoring infrastructure. In addition, YOPP will require comprehensive reference stations on land, sea ice, and in the ocean. The reference sites on sea ice and land could also serve as hubs for wide-ranging observations using, for example, mobile platforms. Extra observations could also be obtained, for example by instrumenting ice breakers and commercial vessels. Additional spot sea ice and upper ocean measurements are of obvious importance as well, and could include mass balance buoys, upward-looking sonar moorings, ice-tethered profilers and ice stress sensors.

One of the key elements of YOPP is to develop a well-coordinated programme that combines a strong observational component with a comprehensive modelling campaign such that the representation of key processes in the Polar Regions in environmental prediction models can be improved. Sea ice models play a key role in environmental prediction by both providing ice products for polar marine users as well as a boundary forcing factor for atmospheric prediction. It is expected that by the time of YOPP a number of coupled and uncoupled ice forecasting systems will be in place producing both deterministic and ensemble ice forecasts. During YOPP it is planned to carry out high-resolution coupled model experiments to explore the benefit of a better representation of key polar processes and significantly enhanced horizontal and vertical resolution.

Given the strong nonlinearities in sea ice physics and the relative few observations available for model development, a coordinated intercomparison in sea ice prediction among operational centres as well as interested research institutions could be of great benefit. This intercomparison could make use of the real-time availability of additional YOPP observations to provide uncertainty estimates for important, yet less well evaluated, fields such as ice pressure, drift and internal temperature. This could provide a means both to highlight best practices (or common errors) as well as to explore the benefits of probabilistic ice forecasting and the potential usefulness of a multi-model sea ice ensemble.

Sea ice is of fundamental relevance to a variety of forecast end users and stakeholders. Consequently, sea ice verification and the usefulness and applicability of spatial verification methods will be in special focus during YOPP. It will also be important to consider additional ice related variables which are relevant to the end users.

Summary and upcoming events

YOPP is an extended period of coordinated intensive observational and modelling activities, in order to improve prediction capabilities for the Arctic, the Antarctic, and beyond. Time scales considered range from hours to seasons, in support of improved weather and climate services, including the Global Framework for Climate Services (GFCS). This concerted effort will be augmented by research into forecast-stakeholder interaction, verification, and a strong educational component. YOPP will provide many early career scientists, including postgraduate students and postdocs, with the opportunity to actively participate in an event that is expected to significantly advance polar research in general, and polar prediction in particular. In order to provide interested students with the necessary background, it is planned to hold at least two ‘Polar Prediction’ summer schools, coordinated with the Association of Polar Early Career Scientists (APECS). The first summer school is planned for 2016 and will be co-organized with WCRP Climate and Cryosphere (CliC) and PCPI projects.

Another upcoming event of interest is a YOPP Summit to discuss planned activities and funding opportunities planned for for July 13-15, 2015 in Geneva. In addition, a workshop on sea ice verification has been tentatively scheduled for March 2016.

A detailed implementation plan for YOPP is available for comment on www.polarprediction.net.

Acknowledgements

We would like to thank the various groups that have commented on and contributed helpful suggestions to the PPP Implementation and Science Plans and the YOPP Implementation Plan.

References

Balmaseda M.A, F. Hernandez, A. Storto, M.D. Palmer, O. Alves, L. Shi, G.C. Smith, T. Toyoda, M. Valdivieso, B. Barnier, D. Behringer, T. Boyer, Y-S. Chang, G.A. Chepurin, N. Ferry, G. Forget, Y. Fujii, S. Good, S. Guinehut, K. Haines, Y. Ishikawa, S. Keeley, A. Köhl, T. Lee, M. Martin, S. Masina, S. Masuda, B. Meyssignac, K. Mogensen, L. Parent, K. A. Peterson, Y. M. Tang, Y. Yin, G. Vernieres, X. Wang, J. Waters, R. Wedd , O. Wang, Y. Xue, M. Chevallier, J-F. Lemieux, F. Dupont, T. Kuragano, M. Kamachi, T. Awaji, A. Caltabiano, K. Wilmer-Becker, F. Gaillard, 2015: The Ocean Reanalyses Intercomparison Project (ORA-IP). J. Operational Oceanogr., accepted.

Bertino L, and Lisæter KA. 2008. The TOPAZ monitoring and prediction system for the Atlantic and Arctic Oceans. J. Op. Ocean., 1(2): 15-18.

Buehner M, Caya A, Pogson L, Carrieres T, Pestieau P. 2013. A New Environment Canada Regional Ice Analysis System. Atmosphere-Ocean, 51(1): 18-34.

Lemieux J-F, Beaudoin C, Dupont F, Roy F, Smith GC, Shlyaeva A, Buehner M, Caya A, Chen J, Carrieres T, Pogson L, DeRepentigny P, Plante A, Pestieau P, Pellerin P, Ritchie H, Garric G, Ferry N. 2015. The Regional Ice Prediction System (RIPS): verification of forecast sea ice concentration, Quart. J. Roy. Met. Soc., accepted.

Johnson, M., S. Gaffigan, E. Hunke, and R. Gerdes. 2007. A comparison of Arctic Ocean sea ice concentration among the coordinated AOMIP model experiments. J. Geophys. Res., 112, C04S11, doi:10.1029/2006JC003690.

Posey PG, Metzger EJ, Wallcraft AJ, Smedstad OM, Phelps MW. 2010. Validation of the 1/12° Arctic Cap Nowcast/Forecast System (ACNFS). Naval Report NRL/MR/7320-10-9287, Stennis Space Center, MS.

Smith, G.C., F. Roy, M. Reszka, D. Surcel Colan, Z. He, D. Deacu, J.-M. Belanger, S. Skachko, Y. Liu, F. Dupont, J.-F. Lemieux, C. Beaudoin, B. Tranchant, M. Drévillon, G. Garric, C.-E. Testut, J.-M. Lellouche, P. Pellerin, H. Ritchie, Y. Lu, F. Davidson, M. Buehner, M. Lajoie and A. Caya. 2015: Sea ice Forecast Verification in the Canadian Global Ice Ocean Prediction System, Quart. J. Roy. Met. Soc.,in review.

IAOOS (Ice - Atmosphere - Arctic Ocean Observing System, 2011-2019)

C. Provost[1] and J. Pelon[2]**, coordinators; **Sennéchael[1], M. Calzas[3], F. Blouzon[3], A. Desautez[4], J. Descloitres[5], work package (co)-leaders, J.C. Gascard[1], N. Villacieros Robineau[1], V. Mariage [2], J.P. Pommereau[2], T. Foujols[2], C. Drezen[3], A. Guillot[3], N. Geyskens[3], N. Amarouche[3], A. Sarkissian[2], N. Pascal[5], M. Garracio[4], P.D. Mahé[3], J. Sayadi[2], J.J. Correia[2], P. Genau[2], N. Wegmüller[6], J-L. Maria[6].

1 UPMC/LOCEAN, Paris, France
2 LATMOS, Paris and Guyancourt, France
3 INSU, Brest and Meudon, France
4 IPEV, Brest, France
5 ICARE, Lille. , France
6 PIT, UVSQ, Guyancourt, France

The key to documenting and understanding change in the Arctic is continuous monitoring. The high cost of Arctic operations thus makes observations by satellite or with long-endurance, refurbishable, autonomous platforms a cost effective solution to continuously observe on-going changes in near real-time. IAOOS (Ice Atmosphere Ocean Observing System, http://www.iaoos-equipex.upmc.fr, http://iaoos.ipev.fr/) is a nine-year France-funded project (2011-2019), developed by LOCEAN and LATMOS, which objective is to provide and maintain an integrated observing system over the Arctic Ocean that collects synoptic and near real time information related to the state of the atmosphere, the snow, the sea-ice and the ocean.

The IAOOS system involves 15 autonomous platforms operating at any given time in the Arctic Ocean for a total period of 5years (2015-2019) and collecting synoptic and near real time information related to the state of the lower atmosphere, the sea-ice and the upper ocean (Fig. 1).

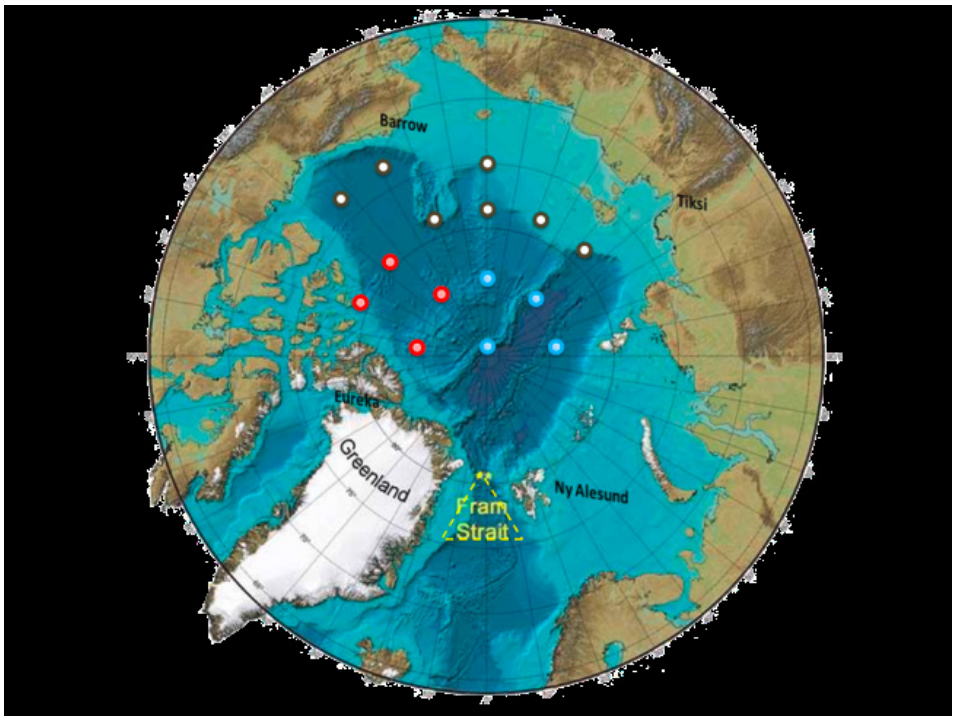

Figure 1: Future distribution of the IAOOS platforms.

Each platform is composed of 3 elements for oceanographic, sea-ice and atmospheric vertical soundings (Fig. 2). Oceanic CTD-DO profilers are derived from the ARGO float except they are tethered to a cable along which they can repeatedly profile vertically from surface down to 800m depth and transmit the data to the surface buoy using an induction modem. An ice mass balance instrument collects sea-ice thickness, snow depth and temperature profiles with a 2 cm vertical resolution across the air-sea-ice-upper-ocean interfaces. The equipment for the atmosphere comprises an autonomous and unattended microlidar and an optical depth radiometer. Standard in situ sensors are used for the measurement of meteorological parameters.

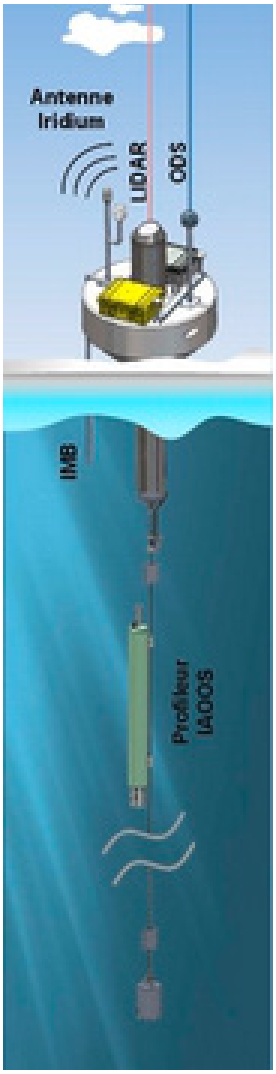

Figure 2: Schematics of a IAOOS platform

The platforms are designed to float at the surface of the ocean as well as to remain on top of sea-ice floes. The target for their autonomy is two years. The fifteen IAOOS platforms will be drifting according to sea-ice motion, surface winds and ocean currents and it will be necessary to replace some of the fifteen platforms every year. It is anticipated that some of the platforms will be either drifting away from the central Arctic Ocean or will be destroyed and lost every year, and some may be recovered in the FRAM Strait. Refurbishing and replacing 5 platforms per year for 2 years following an initial deployment of fifteen platforms will amount to 25platforms for the entire duration of the experiment.

The first three years of the project were devoted to the development and progressive in situ testing of the IAOOS platform prototypes. Major tests were performed deploying more and more complete IAOOS platform at the North Pole in April2012, 2013 and 2014. These platforms drifted from the North Pole in April to Fram Strait (September, October) providing spring summer and autumn field data (Fig. 3). A webcam system supplied information on the environmental conditions and was particularly helpful to interpret the data during the formation and disappearance of a melt pond in July 2013 (Fig. 4).

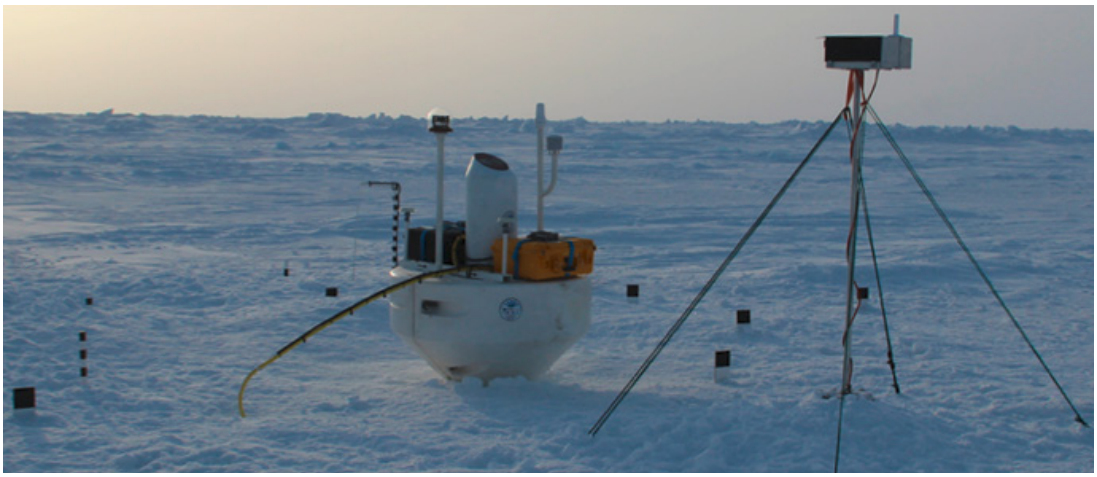

Figure 3: Complete IAOOS platform with microlidar and ODS at the North Pole in April 2014. A web camera is taking pictures 4 times a day to monitor ambient conditions.

Figure 4: IAOOS platform in a melt pond July 26 2013 (picture taken by the webcam)

Important fieldwork for IAOOS is currently taking place within the Norwegian ice camp on board the R/V Lance organized by the Norsk Polar Institute from January to June 2015, as part of the N-ICE 2015, the Norwegian young ICE cruise project. The RV Lance has been allowed to freeze into the sea ice North of Svalbard at 83.25°N and 30°E and is drifting with the ice (Fig. 5)(#NICE2015Arctic on Instagram and Twitter and http://www.npolar.no/en/expedition-field/n-ice2015).
The main scientific objectives of the drift (upper ocean-sea-ice-snow and atmosphere processes and interactions) are detailed in the N-ICE 2015 website. Beyond participating in the scientific objectives of the drift, UPMC-LOCEAN and CNRS-LEGOS+LATMOS scientists are carrying out full testing of the IAOOS platform (Figs 6 and 7) and of the new sensors to be added within the EU-funded project ICE-ARC.
The ice camp is an excellent opportunity to thoroughly proof test the IAOOS platform in winter (so far IAOOS platforms have been tested in spring-summer during drifts from the North Pole to Fram Strait). In the harsh winter conditions, particular attention is paid to the optical windows and lidar calibration for accurate measurements of tropospheric aerosol transported to the pole.

Figure 5 : R/V Lance in the polar night.

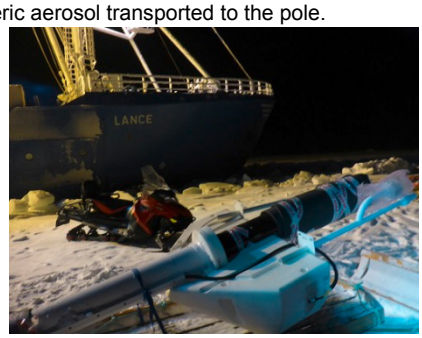

Figure 6: Iaoos platform being prepared on side RV Lance.

Figure 7 : Full IAOOS platform deployed during N-ICE.

The N-ICE camp is also a great opportunity to test new sensors aimed at observing bio-geochemical parameters in the ocean and new radiometry atmospheric sensors in real conditions. Indeed, the ocean Pack RemA including a radiometer, a chlorophyll and CDOM (coloured dissolved organic matter) fluorometer and a backscattering detector has recently been implemented on the IAOOS ocean profiler. In addition, pCO2 and pH sensors will be tested before deciding which sensor to install on the IAOOS platform. Being on the site, scientists have hands on the systems, can test various configurations and gather classical observations and ancillary data for checking data quality and fostering data interpretation.

These intensive tests are very timely. The first IAOOS array deployment will take place from R/V Polarstern during the German cruise TRANSARC II organized by the Alfred Wegener Institute late summer 2015.

SEA ICE ANALYSIS AND FORECASTING WITH GLOSEA5

By K. Andrew Peterson [(1)]

[1] Met Office Hadley Centre, FitzRoy Road, Exeter, EX1 3PB, UK

Abstract

The GloSea5 Coupled Seasonal Forecast System has sea ice fields initialized with the FOAM (GloSea5) ocean and sea ice (re-)analysis system which assimilates SSM/I satellite sea ice concentration observations along with ocean surface and sub-surface observations. We present our seasonal forecast of September sea ice extent emphasizing the problems associated with too thin initial ice thickness conditions.

1. The GloSea5 Seasonal Foraecast System

Seasonal forecasts of sea ice conditions have gained considerable attention in recent years. With the overall decline in Arctic sea ice over the past few decades, the increased economic and socio-environmental interest in the region has a stake in better long term outlooks of sea ice and climate conditions. Research has also suggested links between polar sea ice and climate conditions at mid-latitude [Francis and Vavrus, 2012, and references within], making accurate initialization and forecasting of sea ice a vital tool for seasonal forecasting systems. The Met Office, through GloSea4 [Peterson et al., 2015], was one of the first operational seasonal forecast systems to make use of full dynamically modelled and initialized sea ice in its forecasts.

The latest Met Office seasonal forecast system, GloSea5, has been operational since 16 January, 2013. The system has a 0.25° (ORCA025) resolution version of the NEMO ocean model and CICE sea ice model, coupled to a ~60km version of the Met Office Unified model (UM), and the JULES soil surface model as described in MacLachlan et al. [2014]. Initial conditions for the system are provided for the ocean and sea ice by the Met Office FOAM v13 ocean analysis [Blockley et al., 2014] and for the atmosphere by the Met Office NWP 4D-Var atmospheric analysis. As coupled models invariably have model bias that develops over the course of a 6 month seasonal forecast, a series of historical re-forecasts (or hindcasts) for the 1996-2009 period are run to produce a model climatology by which the forecast can be calibrated and skill derived. For the hindcast, the ocean and sea ice are initialized by the GloSea5 ocean and sea ice analysis, identical to the FOAM system, except for external forcing, which is provided by the ECMWF re-analysis ERA-I, instead of the NWP analysis which FOAM uses, and a changing observational network. The atmosphere for these hindcasts is also initialized with the ERA-I analysis.

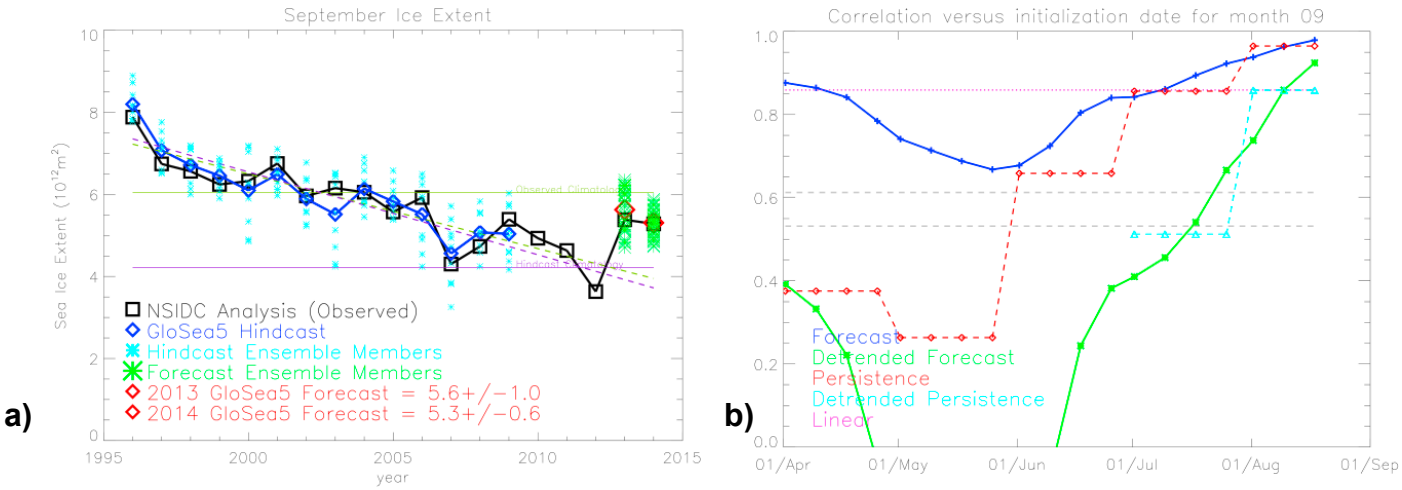

Figure 1: Time series of September ice extents over the hindcast and forecast from the August forecast. The blue's are the ensemble mean bias corrected hindcast values culminating in the 2013 & 2014 ensemble mean forecast (red's). The green/cyan's are the ensemble member sea ice extents from the forecast/hindcast. Black's are the NSIDC observations. b) Correlation skill for September sea ice extent from various start dates. The blue line is full (non-detrended) correlation while the green line is the detrended correlation. The red, cyan, and magenta lines are respectively correlations with full and detrended persistence plus the linear trend.

The ocean and sea ice analysis is performed using the NEMOVAR 3D-VAR assimilation system described in Waters et al. [2014]. The sea ice concentration increments derived from NEMOVAR are inserted into the 5 ice thickness categories of the CICE model as described in Peterson et al. [2015]. Sea ice concentration observations are from the OSI-SAF v2 reanalysis (http://osisaf.met.no) through December 2007, after which the near real time OSI-SAF product is used as in the FOAM system. Observations of sub-surface temperature and salinity, along with sea surface temperature and sea level anomalies are also assimilated.

2. Sea Ice Forecast

The Met Office released an April forecast of September sea ice extent which was subsequently updated in August (http://www.metoffice.gov.uk/research/climate /seasonal-to-decadal/long-range/arctic-sea-ice). Our August update, shown in Figure 1a used forecasts initialized between 22 July and 11 August (42 forecasts, 2 per day), producing an ensemble mean forecast of (5.3±0.6)×1012m2, coincidentally equal to the September 2014 observed value. The forecast was accompanied by 1996-2009 hindcasts initialized on 25 July and 1, 9 August. Correlations between historical observations of sea ice from NSIDC (http://nsidc.org/arcticseaicenews) and the hindcast were 0.94, reducing to 0.74 when the linear trend was removed. The root mean square error over the hindcast was 0.3×1012m2 visually well within the envelope of ensemble variance shown in Figure 1a (each hindcast year had 9 ensemble members, 3 per start date), and also within the quoted error, which was twice the standard deviation of the forecast ensemble members about the ensemble mean. This ensemble spread would be more indicative of the range of possible outcomes rather than our somewhat fortuitous ensemble mean value. At the same time, the bias correction applied to the forecast was 1.8×1012m2 upward. This large value can be traced back to a systematic bias in the analysis of too thin sea ice thickness, which leads to not enough ice surviving the summer melt season. Figure 1b shows why a September ice extent outlook was released using an April forecast followed only by another update in August. The skill of the system takes a precipitous drop in late April, only returning again in July. At the same time, the bias correction, which is quite small for our April forecast (only 0.1×1012m2 downward) rapidly grows positive, quickly becoming the dominant term in forecasts initialized in May through July, a further symptom of the too thin sea ice in the analysis.

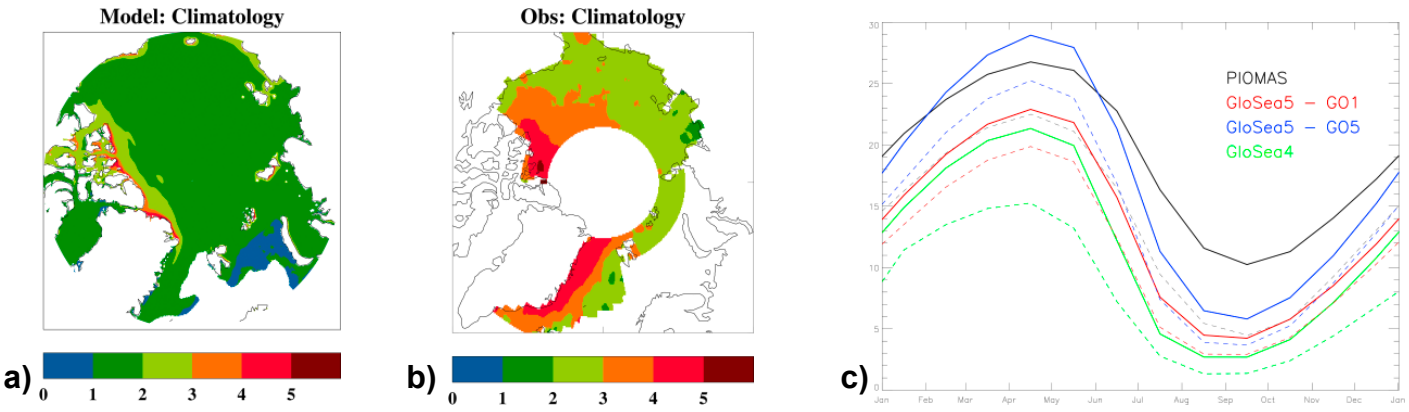

Figure 2: a) Ice thickness climatology of the GloSea5 sea ice analysis for Dec-Mar of 1994-2001. b) Ice thickness from a satellite derived climatology [Laxon et al., 2003] for the same period. c) 1996-2009 mean seasonal cycle of northern hemisphere ice volume in four different analysis: GloSea5 (red), GloSea5-GO5 (blue, operational Feb. 2015), GloSea4 (green) and PIOMAS (black). Dashed lines are seasonal cycle for the analyses in 2011.

Since no satellite observations of summer ice thickness are available, we are only able to make comparisons with winter sea ice thickness. Figure 2 a/b shows a comparison of the Dec-Mar 1994-2001 climatology of GloSea5 sea ice thickness and the satellite derived climatology of Laxon et al. [2003]. It is quite apparent that the GloSea5 analysis ice thickness is too thin. As a further comparison, we compare the seasonal cycle of northern hemisphere ice volume in the GloSea5 analysis with that of the PIOMAS analysis (http://psc.apl.uw.edu/research/projects/arctic-sea-ice-volume-anomaly), an Arctic ice only analysis system. Compared to PIOMAS, the GloSea5 system has considerably lower ice volumes year round. Work has been underway to improve the sea ice state in both the externally forced and coupled sea ice systems, and provisional results for our next analysis are shown with the blue line in Figure 2c. This will be used for operational forecasts starting in February 2015. The GloSea4 analysis used for forecasts in 2011-2013 is shown with the green line.

3. Conclusions

Seasonal forecasting of sea ice remains a challenging problem, largely due to our inability to accurately initialize all aspects of the sea ice using only sea ice concentration observations. Nevertheless, some encouragement is warranted in our ability to skillfully forecast large scale features such as Arctic ice extent. Further progress is being made, which bodes well, not only for seasonal forecasts of sea ice, but also for progress in the seasonal forecasting of European and North American weather [Scaife et al., 2014].

References

E. W. Blockley, M. J. Martin, A. J. McLaren, A. G. Ryan, J. Waters, D. J. Lea, I. Mirouze, K. A. Peterson, A. Sellar, and D. Storkey. Recent development of the Met Office operational ocean forecasting system: an overview and assessment of the new Global FOAM forecasts. Geoscientic Model Development Discussions, 6(4): 6219-6278, 2014. doi: 10.5194/gmdd-6-6219-2013. URL http://www.geosci-model-dev-discuss.net/6/6219/2013/.

Jennifer A. Francis and Stephen J. Vavrus. Evidence linking Arctic amplication to extreme weather in mid-latitudes. Geophys. Res. Lett., page L06801, 2012. doi:10.1029/2012GL051000. URL http://dx.doi.org/10.1029/2012GL051000.

S. Laxon, N. Peacock, and D. Smith. High interannual variability of sea ice thickness in the Arctic region. Nature, 425:947-950, 2003. doi: 10.1038/nature02050.

C. MacLachlan, A. Arribas, K.A. Peterson, A. Maidens, D. Fereday, A.A. Scaife, M. Gordon, M. Vellinga, A. Williams, R. E. Comer, J. Camp, P. Xavier, and G. Madec. Global seasonal forecast system version 5 (GloSea5): a high resolution seasonal forecast system. Quarterly Journal of the Royal Meteorological Society, 2014. ISSN 1477-870X. doi: 10.1002/qj.2396.

K. Andrew Peterson, A. Arribas, H.T. Hewitt, A.B. Keen, D.J. Lea, and A.J. McLaren. Assessing the forecast skill of Arctic sea ice extent in the GloSea4 seasonal prediction system. Climate Dynamics, 44(1-2):147{162, 2015. ISSN 0930-7575. doi: 10.1007/s00382-014-2190-9. URL http://dx.doi.org/10.1007/s00382-014-2190-9.

A. A. Scaife, A. Arribas, E. Blockley, A. Brookshaw, R. T. Clark, N. Dunstone, R. Eade, D. Fereday, C. K. Folland, M. Gordon, L. Hermanson, J. R. Knight, D. J. Lea, C. MacLachlan, A. Maidens, M. Martin, A. K. Peterson, D. Smith, M. Vellinga, E. Wallace, J. Waters, and A. Williams. Skillful long-range prediction of European and North American winters. Geophysical Research Letters, 41(7):2514-2519, 2014. ISSN 1944-8007. doi: 10.1002/2014GL059637.

Jennifer Waters, Daniel J. Lea, Matthew J. Martin, Isabelle Mirouze, Anthony Weaver, and James While. Implementing a variational data assimilation system in an operational ¼ degree global ocean model. Quarterly Journal of the Royal Meteorological Society, 2014. ISSN 1477-870X. doi: 10.1002/qj.2388.

RECENT PROGRESS IN SEA ICE DATA ASSIMILATION AT ENVIRONMENT CANADA

By M .Buehner[(1)], A. Caya[(1)], M. Ross[(2)], Y. Luo[(3)], T. Carrieres[(3)], L. Pogson[(3)]

[1] Data Assimilation and Satellite Meteorology Research Section, Environment Canada, Dorval, Canada
[2] RER Energy Inc., Montreal, Canada
[3] Canadian Ice Service, Ottawa, Canada

Abstract

This brief report describes the current configuration of the analysis component of the Environment Canada Regional Ice Prediction System and recent research results from the assimilation of high resolution visible/infrared satellite data.

Current sea ice data assimilation system

A series of improvements were recently implemented for the ice concentration analysis system that represents the analysis component of the Canadian Regional Ice Prediction System (RIPS; Buehner et al., 2014). In addition, the domain of the system was enlarged to cover all of the Arctic Ocean, whereas the previous system only included the waters around North America and the portion of the Arctic Ocean extending until just beyond the North Pole. The system is primarily aimed at supporting the Canadian Ice Service (CIS) operational activities for ice affected waters around North America. It also provides the initial ice concentration field for the forecast component of RIPS, which has recently been implemented operationally to produce 48 h forecasts of ice conditions. The system is based on the three-dimensional variational data assimilation approach (3D-Var). Initial developments are described in detail by Caya et al. (2010) and Buehner et al. (2013). A brief description of the current system is given in the remainder of this section.

Only ice concentration is estimated on a grid with ~5 km spacing four times (valid at 0, 6, 12, and 18 UTC) each day. The assimilation algorithm is known as 3D-Var in which the gridded sea ice concentration analysis is the value of **IC** that minimizes the cost function:

$$J(\mathbf{IC}) = \frac{1}{2}\left(\mathbf{IC}-\mathbf{IC}^{b}\right)^{T} B^{-1}\left(\mathbf{IC}-\mathbf{IC}^{b}\right) + \frac{1}{2}\left[y-H(\mathbf{IC})\right]^{T} R^{-1}\left[y-H(\mathbf{IC})\right] \quad (1)$$

where IC^b is the ice concentration background state, **y** is the vector of observed values, *H* is the observation operator that transforms the gridded ice concentration into quantities that are directly comparable with the observations, **R** is the observation-error covariance matrix, and **B** is the background-error covariance matrix. All observations within a 6 h assimilation time window are considered when producing the analysis at the centre of the window. There is currently no sea ice model used in the data assimilation cycle, but instead the previous analysis is used as the background state. As an additional step, the ice concentration in the analysis is set to zero for all grid points where the sea surface temperature (SST), obtained from a separate SST analysis system (Brasnett, 2008), is above 4°C.

Ice concentration derived from the passive microwave observations of the Special Sensor Microwave/Imager (SSM/I) and Special Sensor Microwave Imager Sounder (SSMIS) are assimilated. The retrieved ice concentration is calculated using the NASA Team 2 (NT2) sea ice algorithm (Markus and Cavalieri, 2000). The footprint sizes of the passive microwave channels used are significantly larger than the grid spacing of the analysis. To avoid contaminating small scale details that are not represented in these observations, a so-called “footprint operator” is used as part of the observation operator. This footprint operator averages the gridded ice concentration over all grid points within a distance from the observation location equal to the footprint radius of the sensor, thus simulating the spatial averaging effect of the actual satellite measurement. An important quality control procedure is applied that rejects all observations where the surface air temperature (obtained from the Canadian operational weather prediction system) is above zero. This is necessary to reduce the negative impact of the large biases in NT2 ice concentration retrievals from passive microwave data that occur when the ice or snow surface becomes wet or covered by ponds from surface melting.

Data from the active radar scatterometer instrument ASCAT are also assimilated. These data are in the form of three measured backscatters made from three distinct look angles for each location on the surface. As with passive microwave data, a footprint operator is used as part of the observation operator when assimilating ASCAT data. Most of the ASCAT data are assimilated after being converted into a single measure of backscatter anisotropy at each location, following Breivik et al. (2012). The basic idea of assimilating a derived measure of backscatter anisotropy is that over open water the wind creates capillary waves that cause the amplitude of the three backscatters to differ from each other depending on the orientation of the waves with respect to the three look directions. On the other hand, over ice the three backscatters tend to have relatively similar amplitudes, since the scattering is more random. The remainder of the assimilated ASCAT data is in those locations where several criteria computed from the backscatter data indicate that open water is present. At these locations a 0% ice concentration value is assimilated directly. This avoids introducing small non-zero ice concentration values over areas where there is very likely no ice.

Also assimilated is the ice concentration derived from several types of ice analysis products prepared manually by CIS. This includes the daily ice charts (Carrieres et al., 1996) that are subjective nowcasts of the instantaneous ice concentration valid at 18 UTC based on several types of remotely sensed and other available data. In addition, CIS subjectively analyzes individual synthetic aperture radar (SAR) images, mostly from RADARSAT-2, to derive ice type distributions including estimates of total ice concentration. Both of these types of ice charts cover a relatively small portion of the RIPS domain that varies according to the season. Finally, weekly analyses of ice concentration for a large number of small lakes within Canada are also assimilated.

Due to the relatively low spatial resolution of the satellite data assimilated in RIPS as compared with the analysis grid resolution and the incomplete coverage of the CIS ice charts, the estimated ice concentration at many grid points near the coast and in narrow channels and bays is not directly influenced by any observations. This is because all satellite observation footprints that contain any land are rejected since the presence of land can cause spurious values of retrieved ice concentration. To reduce the impact of this type of error, a procedure was implemented for estimating the

uncertainty of the RIPS ice concentration analysis at each grid point. The procedure is roughly based on Kalman filter theory, such that the uncertainty is reduced during the analysis step, depending on the number and relative accuracy of the assimilated observations near a particular grid point, and the uncertainty is increased during the forecast step. The net effect is that grid points in narrow channels and bays have a high estimated analysis error stddev because of the lack of nearby assimilated observations, whereas other locations with recently assimilated observations have a much lower analysis error stddev. This estimated analysis error stddev is then used to identify grid points that should be considered highly uncertain using an empirically chosen threshold value of 0.6. For all of these identified grid points the ice concentration estimates are replaced with values obtained from applying an interpolation/extrapolation procedure that spreads the information from nearby grid points where the uncertainty is lower. As a result, the ice concentration analysis in narrow channels and bays are actually computed from the values at grid points just adjacent to these areas where a sufficient number of observations were recently assimilated. This approach improves the average accuracy of the estimated ice concentration field, though in some situations the replaced values lead to a local degradation in accuracy. Regardless, this procedure is a temporary solution, since the eventual assimilation of higher resolution observations and observations less sensitive to surface melting will reduce the uncertainty for most areas and therefore reduce the number of grid points where this procedure is applied.

Towards the assimilation of high-resolution visible/infrared data

To further improve the quality of the ice concentration analyses produced by RIPS, research is underway to effectively assimilate information from high resolution remote sensing data in a completely automated manner. This includes data from both SAR and visible/infrared instruments. In the remainder of this section a brief summary is given of preliminary results from using visible/infrared data from AVHRR which has a resolution of approximately 1.1 km. The specific goal is to improve the analyses in areas not observed by passive microwave and scatterometer observations due to their large footprint size, that is, near the coast and in narrow channels and bays. This work builds on the earlier study by Scott et al. (2013).

A major challenge with using data from visible/infrared instruments is the need to efficiently identify those observations affected by clouds or fog so that they can be eliminated. Locations where clouds are not rejected can result in spurious ice being introduced in the RIPS analysis where there should be none. To reduce the computational expense, the AVHRR observations are first averaged to a 5.5 km grid, which is similar to the resolution of RIPS. A geolocation correction of AVHRR imagery is then applied by using ground control points based on clear-sky MODIS images. An initial screening of clouds is performed by using a modified version of the SPARC algorithm (Khlopenkov and Trishchenko, 2004). Then, a series of thresholds are applied to the data based on the channel 1 reflectance (Ch1R) and the channel 3B reflectance (Ch3BR) to classify each pixel (as shown in Figure 1). This classification procedure further removes pixels that are likely affected by clouds. The data classified as ice and water are then assimilated in the 3D-Var as 100% and 0% ice concentration, respectively, in combination with all of the data already used in RIPS (as described in the previous section). AVHRR data are only used between 1200UTC and 2359UTC, since very little data on the ascending node of the orbit is available with sufficient solar illumination outside of this period. The lack of solar illumination is clearly a limitation of visible/infrared data, however in the current system the largest sea ice concentration errors occur during summer when this is less of a limitation. Indeed the largest positive impact from assimilating AVHRR data is obtained during summer. Most of this improvement results from introducing open water in areas that were previously covered with ice. An example is given in Figure 2 showing the RIPS ice concentration analysis on 31 July 2011 at 1200UTC from an experiment with only the observations described in the previous section (left panel) and an experiment that additionally assimilated AVHRR data (right panel). There is a clear reduction in ice concentration near the coasts from assimilating AVHRR data and this is generally more consistent with the CIS regional ice chart (Figure 3; note that the regional charts are not assimilated in RIPS and often cover areas not covered by daily ice charts or SAR image analysis charts).

These preliminary results show the potential positive impact on the RIPS analyses. Research is continuing to further improve the detection of clouds. We are also exploring improved approaches for assimilating the ice/water classified data in 3D-Var and beginning the work to apply the same approach to VIIRS data. The VIIRS instrument is a recent visible/infrared sensor which provides a higher spatial resolution, more channels (which should improve cloud detection), a wider swath, and more accurate georeferencing than AVHRR.

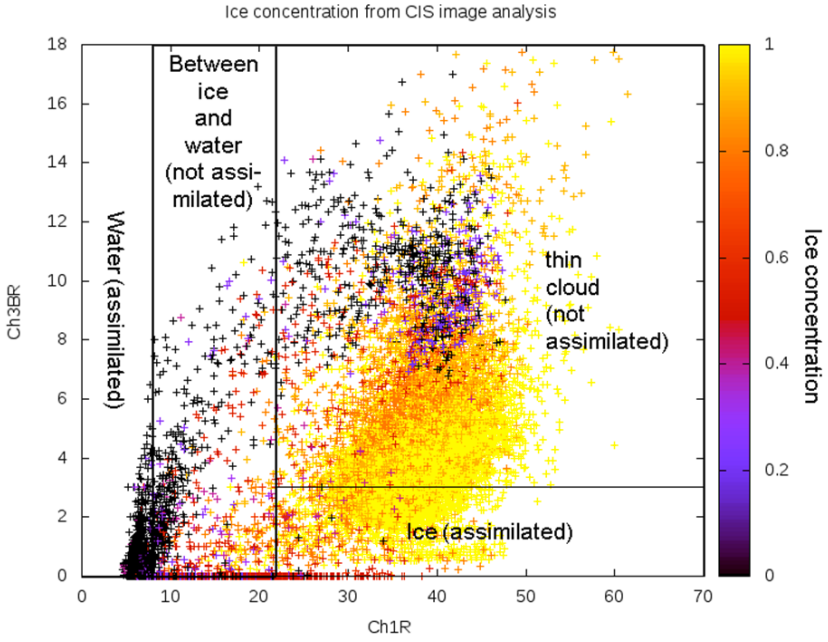

Figure 1: Illustration of the classification approach applied to AVHRR channel 1 reflectance (Ch1R) and channel 3B reflectance (Ch3BR). The vertical and horizontal lines denote the thresholds used to identify areas likely to be either covered by ice (bottom-right rectangle) or water (left-most rectangle) and not affected by clouds. The coloured '+' symbols indicate a set of AVHRR observations co-located with a CIS image analysis where the colour indicates the concentration from the image analysis.

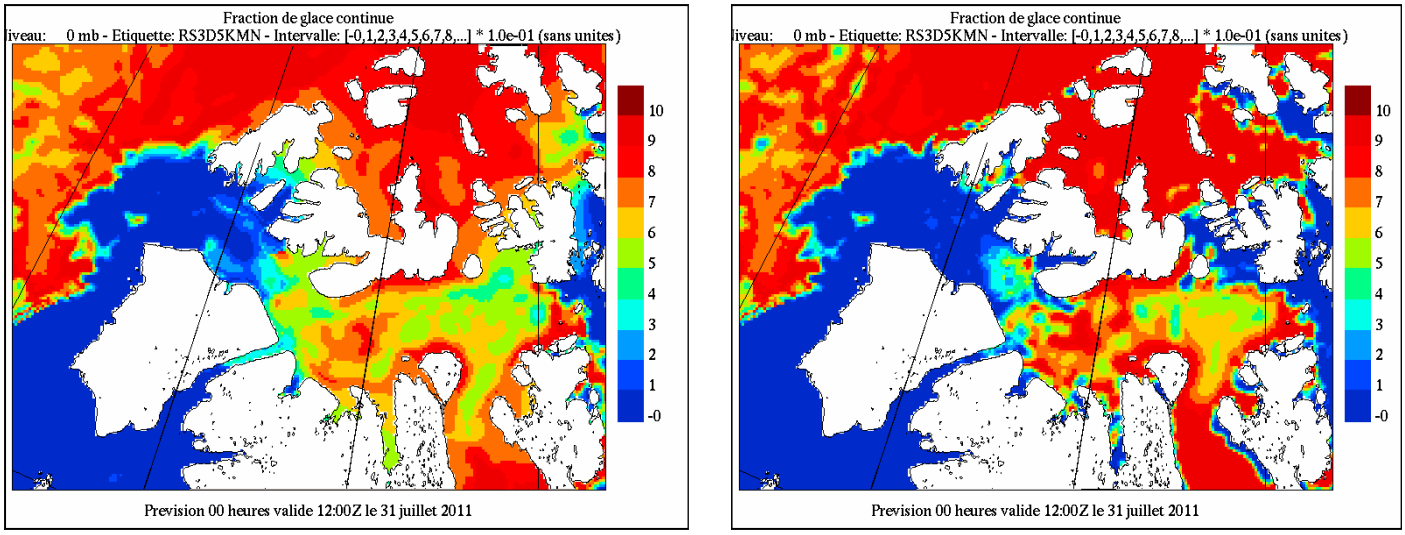

Figure 2: Ice concentration analysis in a portion of Canadian Arctic Archipelago from RIPS, valid on 31 July 2011 at 1200UTC. Left: when only the passive microwave, scatterometer and CIS manual analysis data are assimilated. Right: when AVHRR data are assimilated in combination with the same data assimilated as in the left panel. The units used for the colour bar are tenths.

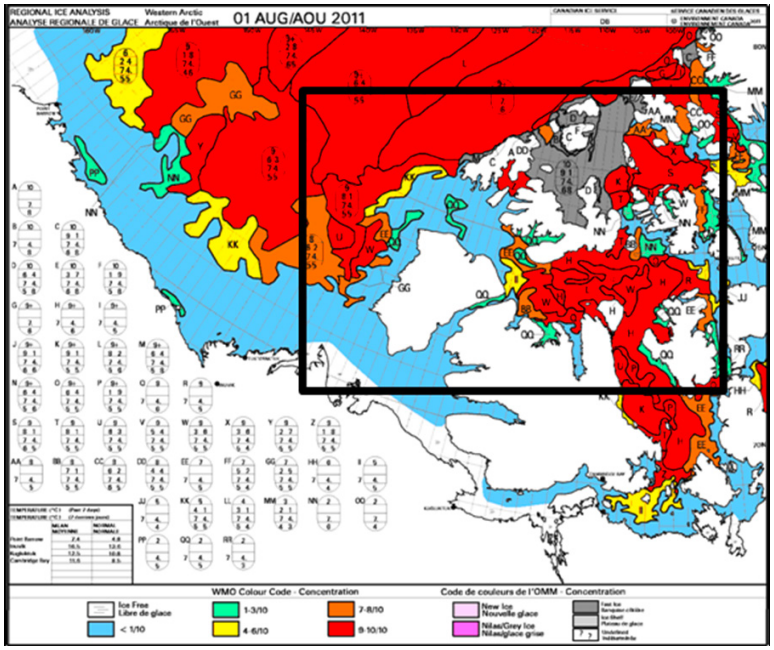

Figure 3: The CIS regional ice chart ice concentration valid on 1 August 2011. The region indicated by the black rectangle approximately corresponds with the area shown from the RIPS analyses in the previous figure.

Other ongoing research

In addition to the assimilation of high resolution visible/infrared data, work is also being performed in other areas to improve RIPS. These include: assimilation of ice concentration retrievals from AMSR-2, fully automated assimilation of SAR data, assimilation of ice thickness data (e.g. from SMOS), and the use of a numerical sea-ice model within the data assimilation cycle. In addition, preliminary research is being conducted to explore the use of ensemble methods, both to improve the data assimilation system and to provide probabilistic products based on ensembles of analyses and forecasts.

Acknowledgements

The authors wish to thank the organizers of the 6th International Workshop on Sea Ice Modelling and Data Assimilation that took place in Toulouse, 15-16 September 2014.

References

Brasnett, B. 2008: The impact of satellite retrievals in a global sea-surface-temperature analysis. Q. J. R. Meteorol. Soc. 134:1745–1760.

Buehner M., Caya A., Pogson L., Carrieres T. and Pestieau P. 2013: A New Environment Canada Regional Ice Analysis System. Atmosphere-Ocean 51:18–34.

Buehner, M., Caya, A., Carrieres, T. and Pogson, L. 2014: Assimilation of SSMIS and ASCAT data and the replacement of highly uncertain estimates in the Environment Canada Regional Ice Prediction System. Q. J. R. Meteorol. Soc. doi:10.1002/qj.2408 (Early View online version)

Breivik, L.-A., Eastwood, S., Lavergne, T. 2012: Use of C-Band Scatterometer for Sea Ice Edge Identification. IEEE Trans. Geos. Rem. Sensing 50:2669–2677.

Carrieres, T., Greenan, B., Prinsenberg, S. and Peterson, I.K. 1996: Comparison of Canadian ice charts with surface observations off Newfoundland, winter 1992. Atmosphere-Ocean 34:207–236.

Caya, A., Buehner, M. and Carrieres, T. 2010: Analysis and Forecasting of Sea Ice Conditions with Three-Dimensional Variational Data Assimilation and a Coupled Ice–Ocean Model. J. Atmos. Oceanic Technol. 27:353–369.

Khlopenkov, K. and Trishchenko, A. 2004: SPARC: New cloud, snow and cloud shadow detection scheme for historical 1-km AVHRR data over Canada. J. Atmos. Oceanic Technol. 24:322–343.

Markus, T. and Cavalieri, D.J. 2000 : An enhancement of the NASA team sea ice algorithm. IEEE Trans. Geos. Rem. Sensing 38:1387–1398.

Scott, K.A., Buehner, M., Caya, A. and Carrieres, T. 2013: A preliminary evaluation of the impact of assimilating AVHRR data on sea ice concentration analyses. Remote Sensing of Environment 128:212–223.

RECENT DEVELOPMENTS IMPACTING THE SEA ICE IN THE MERCATOR OCÉAN GLOBAL ¼° CONFIGURATION.

By G. Garric[1], C. Bricaud[1], L. Chateigner[2], J. Tournadre[3], M. Vancoppenolle[4], C. Rousset[4]

[1] Mercator Océan, Ramonville Saint-Agne, France
[2] Météo France, Toulouse, France
[3] IFREMER/CERSAT, Brest, France
[4] Sorbonne Universités (UPMC Paris 6), LOCEAN-IPSL, CNRS/IRD/MNHN, Paris, France

Introduction

With a large freshening of the upper Arctic Ocean, the thinning of the Arctic sea ice cover and the important melting of continental ice sheets, high latitudes undergo important and rapid changes. To better understand these changes and their impact on the ocean as simulated in hindcasts, nowcasts and forecasts simulations, it is desired to improve the representation of both: sea ice processes and the release of fresh water by melting ice sheets and icebergs. In particular, these processes likely impact the dynamical and thermohaline processes affecting the formation of water masses at a global scale. With this long-term overarching goal in mind, Mercator Ocean, the French operational oceanography center, has tested two main developments in the NEMO-based model component in its global 1/4 ° reanalysis system: (i) the multi-category LIM3 sea ice model and (ii) the comprehensive representation of the freshwater flux from polar ice caps. This short paper gives a quick overview of the impact of using LIM3 instead of LIM2 on the modeled sea ice cover in part 1 and of the method used to build the freshwater forcing from continental ice sheets and an idealized impact on sea ice cover in part 2.

Multi-category sea ice model: LIM3

The new version of Louvain-La-Neuve sea ice model LIM3 (Vancoppenolle et al, 2009) is now available in the standard version 3.6 of NEMO (Madec, 2008), together with the previous version LIM2 (Fichefet and Morales Maqueda, 1997; Timmermann et al., 2005). LIM3 is now the base for future developments and LIM2 will be discontinued within a two-year horizon. The main differences between LIM2 and LIM3 can be summarized as follows:

- **Thermodynamics (heat diffusion, growth and melt).** LIM2 uses the Semtner (1976) 3-layer model, with pure ice thermal properties and a latent heat reservoir emulating brine inclusions. Ice-ocean exchanges of freshwater and salt are computed assuming a prescribed ice salinity. LIM3 uses an improved multi-layer representation in the vein of the Bitz and Lipscomb (1999) model. The thermal properties depend on brine volume fraction, which is a function of salinity and temperature. Exact conservation of heat, salt and water is ensured (Rousset et al., in prep). The bulk salinity changes due to uptake during growth and rejection by brine drainage, and the vertical salinity profile is parameterized as a function of the bulk salinity (Vancoppenolle et al., 2009b). The transition from LIM2 to LIM3 thermodynamics involves slight changes in the seasonality of ice volume (Vancoppenolle et al., 2009b) and more robust ice-ocean exchanges than in LIM2, in particular near river mouths, in low-salinity seas and in weakly stratified systems such as the Southern Ocean. Both LIM2 and LIM3 include the same simple snow thermodynamics, and the conversion of snow into ice (snow-ice formation).
- **Ice thickness distribution.** Ice thickness is highly variable at subgrid scales, which is important to account for since both growth and melt depend non-linearly on thickness. LIM2 emulates the representation of subgrid-scale ice thickness variations, in particular thin ice by (i) enhancing the thermal conductivity of snow and ice and (ii) increasing the reduction of ice concentration associated with melting. In LIM3, the statistical distribution of ice thickness is explicitly resolved, using a variable number of thickness categories (typically 5), which discretize the ice thickness distribution (Thorndike et al., 1975). Ice categories exchange ice area and volume (and all other state variables such as heat and salt content) due to ice growth, melt, ridging and rafting.
- **Dynamics.** Both LIM2 and LIM3 use the same dynamical core. The sea ice momentum equation is solved using the C-grid Elastic Viscous Plastic (EVP) method (Bouillon et al, 2013), with the ice strength formulation of Hibler (1979), combined with a 2nd order momentum conserving advection scheme. A notable dynamical difference between LIM2 and LIM3 is the representation of mechanical deformation on ice thickness. In LIM2, ridging is implicitly represented by preventing the ice concentration to exceed 100% in a volume-conserving way. In LIM3, the impact of porous ridging and rafting on the ice thickness distribution is explicitly represented.

The first goal of this study was to assess the LIM3 implementation in a global ¼° context and to evaluate main differences to the LIM2 version. Two inter-annual 1979-2009 experiments were performed with the Mercator global ¼° configuration, one with LIM3 and the other with LIM2. The ¼° configuration is based on the tripolar ORCA grid type, featuring a horizontal resolution of less than 20km in the Arctic Ocean and the Nordic Seas, and 75 vertical z-levels (1m resolution at the surface decreasing to 200m at the bottom), Lellouche et al. (2014) explain further details on the physics retained in this configuration. Both experiments are driven at the surface by the ERA-Interim reanalysis (Dee et al., 2011). A 3-hour sampling for surface air temperature, humidity and wind is used to reproduce the diurnal cycle. An analytical formulation is applied to the daily mean shortwave flux in order to reproduce an ideal diurnal cycle. A large scale correction is applied to radiative and rainfall fluxes towards respectively Gewex-SRB and GPCPV2.2 satellite data. Surface air temperature and relative humidity are corrected over the Arctic sea ice in summer based on Lüpkes et al. (2010) and Jakobson et al. (2012) assessments. The model is initialized as follows: temperature and salinity with Levitus et al. (1998), sea ice concentration with Defense Meteorological satellite Program-F17 Special sensor Microwave Imager/Sounder (DMSP SSM/I-SSMIS) passive microwave data (Comiso, 2000) and sea ice thickness from a mean 1985-1990 January 1° global Mercator configuration experiment performed with the LIM2 sea ice model.

To assess the realism of the simulated sea ice concentration, we compare the two experiments to an ensemble of satellite observations from four sources: IFREMER/CERSAT (French Research Institute for Exploitation of the Sea / Centre ERS d'Archivage et de Traitement, Ezraty et al., 2007),

EUMETSAT Ocean and Sea Ice Satellite Application Facility (OSI-SAF, 2011), National Snow and Ice Data Center (NSIDC, Comiso, 2000) and European Space Agency – Climate Change Initiative (ESA-CCI, Kern et al., 2015) . The spread of the ensemble is defined by the range between the minimum and the maximum observed values in the four data sets. Correlations among data sets cannot be ignored since these data sets employ similar raw passive microwave radiances, and the conversion algorithms share some similarities. Nevertheless, the envelope gives an approximation of ice concentration uncertainties in satellite concentration retrievals. We focus our comparison on the Arctic Ocean as an error has been introduced in the atmospheric forcing field that prevents a reasonable and fair comparison between LIM2 and LIM3 experiments in the Southern Hemisphere.

The sea ice concentration output from the LIM3 experiment is contained within the observational spread over the whole annual cycle and is close to the mean observations estimates during the last half of the year. In contrast, the output from LIM2 overestimates during summer and fall (Figure 1). This finding is particularly relevant as satellite retrievals are known to underestimate the extent of ice during summer due to the presence of melt ponds. However, LIM3 seems to predict the spring maximum one month in advance compared to LIM2 and the observed mean estimate. This one month phase shift is also present during summer in the annual cycle of the sea ice fraction (Figure 1) where LIM3 shows a minimum in August instead of September. LIM3 also shows larger amplitude of the seasonal cycle than LIM2. The overestimation found during winter in LIM3 is mainly found in the peripheral seas such as the Bering, Labrador and Okhotsk seas (not shown). However, considering the 50% contours of ice fraction shown in Figure 2, LIM3 and LIM2 are close to the mean satellite estimates during winter. During summer, LIM3 exhibits an important reduction of sea ice extent compared to LIM2 which gives a better mean state compared to the mean observed estimates. This reduction is found principally in the Western part of the Arctic basin where both model versions exhibit an unrealistic accumulation of sea ice. The mean sea ice thickness formed by LIM3 is thicker than that formed by LIM2 in all seasons (not shown). Compared to the ICESat thickness distribution in winter 2007 (Kwok et al., 2009), the LIM3 experiment shows a more realistic distribution of mean sea ice thickness along the northern part of the Canadian Archipelago together with a substantial thinner and more realistic (still compared to ICESat) ice thickness in the Western part of the Arctic basin (Figure 3). Almost no differences in the interannual variability are observed between the two experiments (not shown).

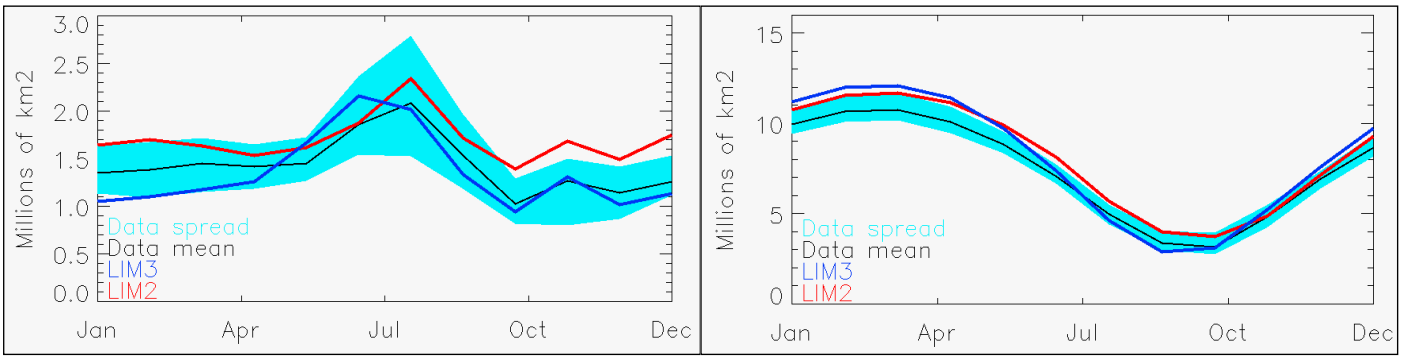

Figure 1: Mean 1992-2009 annual cycle of leads (the total open water area in regions with at least 15% concentration of ice) (left) and sea ice extent (defined as the area enclosed within the 15% concentration contour of ice) (right) both expressed in millions of km2 for Northern Hemisphere. LIM2 is in red and LIM3 in blue. Dark line and blue envelop denote the mean and spread of four satellite estimates (NSIDC, CERSAT, OSI-SAF and ESA-CCI).

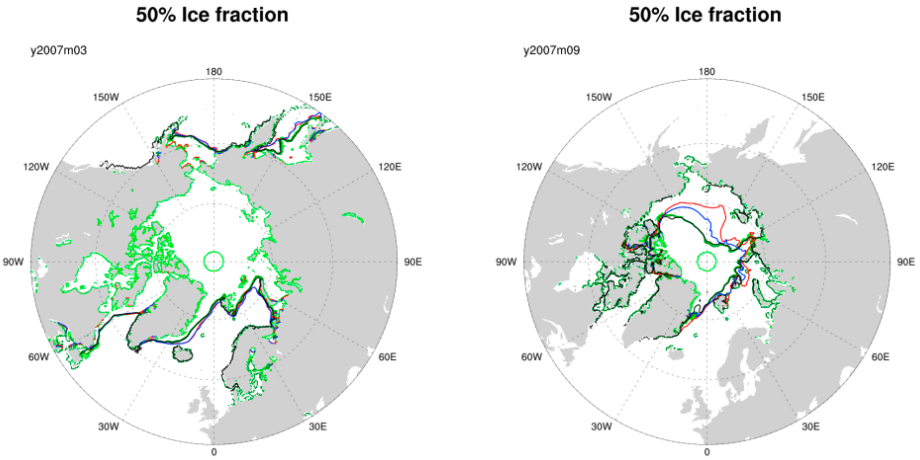

Figure 2: 50% ice fraction contour for March 2007 (left) and September 2007 (right) for the mean ensemble (OSISAF, ESA-CCI, NSIDC, CERSAT) satellite products (green), LIM2 (red) and LIM3 (blue). Despite the year 2007 shows an historical minimum record in summer, this year indicates the general findings in 30 years of the experiments.

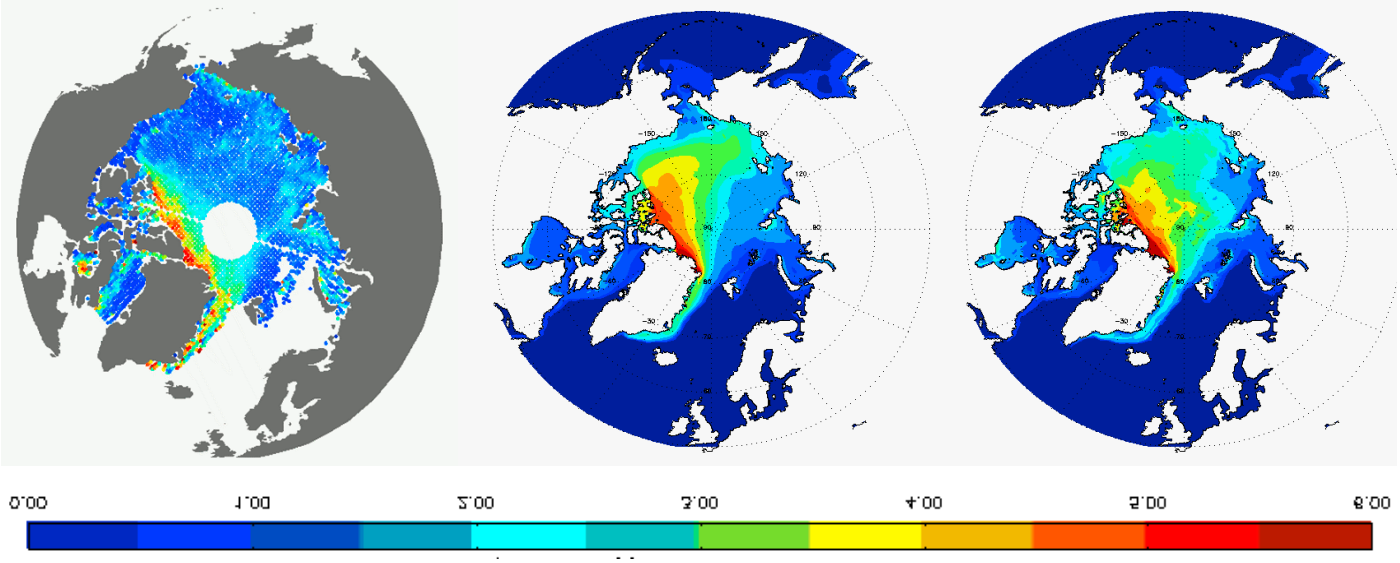

Figure 3: Sea Ice thickness for March 2007 from ICESat (left); for LIM2 (middle) and for LIM3 experiments (right).

Freshwaters fluxes from polar ice caps melting

Recent reconciled estimates point out that mass losses from Greenland and Antarctica ice sheets have increased rapidly over the last two decades (Shepherd et al., 2012) and are likely to become one of the main contributors to the global sea level rise (Church et al., 2013). However, reconstructions of the recent decades with Oceanic General Circulation Models (OGCMs) are usually made with crude representations of freshwater forcing from polar ice sheet melt. Presently, also Mercator's configurations use in their analysis and forecast systems a simple approach with a seasonal climatology from Silva et al. (2006) for the Antarctic ice sheets and a speculative signal for the Greenland ice cap from Dai and Trenberth (2002). In order to better represent the variability in the freshwater flux from continental ice sheets entering the future analysis system, we have applied a simple method to build a comprehensive interannual polar ice cap forcing over the altimeter era. This freshwater forcing is based on the Altiberg icebergs project dataset (Tournadre et al., 2012), the Gravity Recovery and Climate Experiment (GRACE)-based ocean mass signal (Ramillien et al., 2006) and the IPCC's Fifth assessment Report (Church et al., 2013). We proceed in several steps to construct this data set:

- We first use the Altiberg database to estimate the interannual variability and the phase of the seasonal cycle of the mass loss from the Greenland and the Antarctic ice sheets. The aim of Altiberg (Tournadre et al., 2008) is to identify surface, volume and frequency of small icebergs (1-2 Km) in both Southern and Northern Hemisphere (SH and NH hereafter) from radar altimeter measurements. The method uses a parabolic signature in the radar altimeter waveform analysis to identify small icebergs. Monthly maps of icebergs detections and surface distributions are merged from all altimeters operating between 1993 and 2012. All iceberg features are given on a regular polar grid at a resolution of 1°x2°. To evaluate the interannual annual freshwater flux from the iceberg volume, all icebergs are assumed to melt entirely in one year. Then, the annual flux is sampled monthly using a ratio between the volumetric budget of two successive months and the difference between the maximum and minimum volume observed during the year.
- The ice sheet mass loss is driven by the liquid runoff due to surface melting and runoff and the solid ice discharge from outlet glaciers. Even if the relative share of the solid ice discharge on the total loss seems to weaken during the recent years (Enderlin et al., 2014), liquid and solid relative contributions are still under debate. According to previous studies (Rignot et al., 2008 and Silva et al., 2006), we have used a constant relative share and have considered iceberg calving to represent about a third of the total ice sheet melt.
- Different methods for the two polar ice caps are used to estimate the spatial (coastal) distribution of the liquid part of the runoff. Due to the limitations of the coverage of observation from altimeters (Jason), the volume of icebergs in the Weddell and Ross Seas south of 66°S is estimated from the climatology of the large tabular icebergs from Silva et al. (2006). Together with a uniform distribution at the Antarctica coast, these contributions are assumed to represent the liquid part of the total signal. In the NH, there are only relatively small icebergs and no climatology exists. We apply a polynomial regression on estimations made by Rignot et al. (2008) on particular years (1996, 2000 and 2005) to adjust annual mass losses of the Greenland ice sheet over the 1993-2012 period. Then, mass losses are distributed along the Greenland coast according to climatological 2002-2008 gravity field intensity anomalies measured by GRACE.
- We have also adjusted the amplitude of the seasonal cycle (annual mean) and the tendencies of the total signals to the AR13 IPCC values' (Church et al. 2013) (See Table 1).

	Greenland	Antarctica
Trend 1993-2001	0.09	0.08
Trend 2002-2012	0.59	0.4
Trend 1993-2012	0.38	0.27
Annual Mean	2.12 (1993-2012)	4.43 (1993-2012)

Table 1: Linear trend and annual mean in mm.yr-1 used in the experiment ICE_SHEET.

The spatial distribution of icebergs identified by Altiberg is shown in the annual mean of the resulting freshwater flux in Figure 4. For both hemispheres, maxima are generally found along the coast, at the vicinity of important glaciers (e.g. Jakobshavn in Greenland) or along ice shelves in Antarctica. In the Southern Ocean, the patterns of the distribution with three well-defined maxima, one in each ocean corresponds to the general iceberg circulation. The main surface currents (the components of the northern sub-polar Gyre, i.e. the East, West, Baffin Island and Labrador currents) transport them out of their calving sources in the NH. It has to be noted that Altiberg also identified the icebergs calved from eastern Canada glaciers. The amplitude of the seasonal cycle is larger in the SH than in the NH with a peak value in January for the SH. The number of icebergs is also larger in the SH than in the NH by a factor of 4 to 5 due in large part to deterioration of sporadic large tabular iceberg calving from Antarctic ice sheets, the seasonal cycle in the SH exhibits a very large inter-annual variability (much larger than in the NH) (Figure 5).

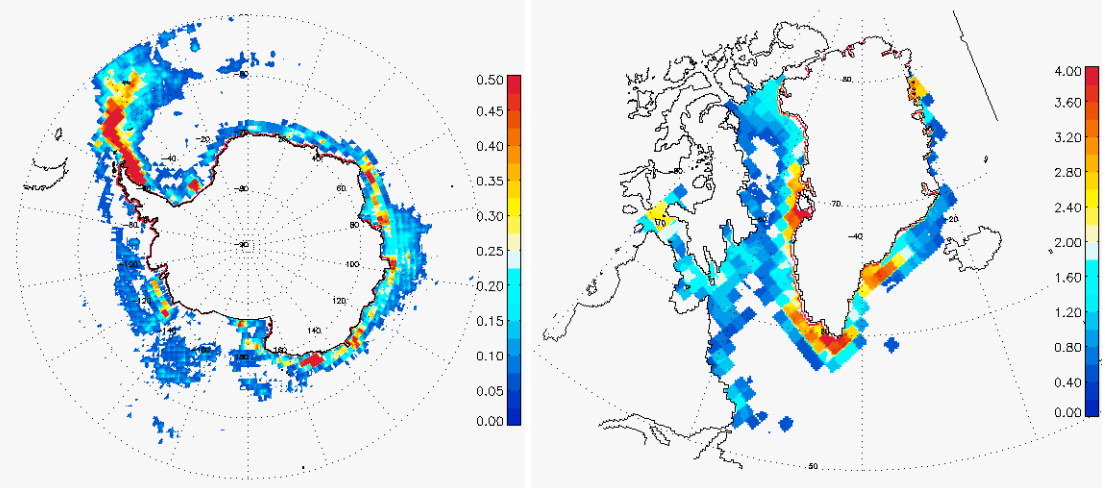

Figure 4 : 1993-2012 mean annual freshwater flux in mm.yr-1 (x 100000).

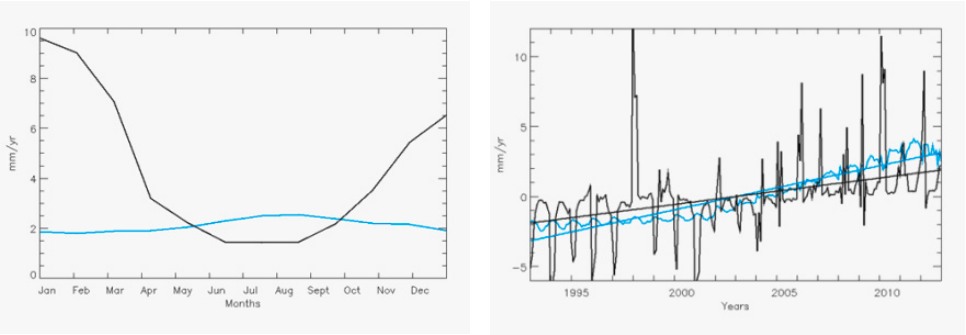

Figure 5: Mean (1993-2012) annual cycle of freshwater flux (mm/year) (left) for NH (Blue) and SH (black). Freshwater flux (mm/year) anomalies (from 1993-2012 climatology) for NH (blue) and SH (black). Linear tendencies are superimposed on each curve.

Two experiments have been performed in the 1993-2012 period with the global ¼° configuration of Mercator-Ocean, based on NEMO and LIM2 briefly described in the previous part. The first experiment is a control experiment with no ice sheet melt (hereafter REF) whereas the second experiment (hereafter ICE_CAPS) uses the new freshwater forcing. We subsequently assess a major sensitivity impact of a realistic continental ice sheet melting on the oceanic circulation and water mass distribution. The freshwater forcing is implemented at the surface as a precipitation flux. The extra freshwater input into the upper layer of the ocean modifies the surface waters density by drastically reducing the salinity, e.g. the salinity can decrease locally by up to 1 PSU on average (not shown). The reduction of surface water density stratifies the upper ocean and stabilizes it. The mixed layer depth can reduce up to 1000m in the northern Sub Polar, Weddell and Ross Seas Gyres during winter (not shown) and by 200m on average. A weaker deepening of the mixed layer depth is also observed in the core of each gyre. We speculate that this feature is due to dynamical vertical mass adjustments. This impacts on the sea ice cover in the SH significantly (Figure 6). The shallowing of the mixed layer depth more efficiently insulates cold surface waters from warmer waters found in deeper layers in the Southern Ocean. These colder surface waters foster the formation of sea ice. Positive concentration anomalies of up to 40% can be reached with an almost simultaneous thickening of up to 40cm along the coast of Antarctica. The Figure 6 also reveals a weakening of ice fraction in areas (core of the Weddell Gyre) where the mixed layer deepens and brings warmer water to the surface. No significant effects are observed on sea ice cover surrounding Greenland. These extra freshwater releases are also strongly influencing the global large scale circulation, slowing down the Northern Sub-Polar, the Weddell and the Ross seas Gyres and the Atlantic Meridional Overturning Circulation (not shown).

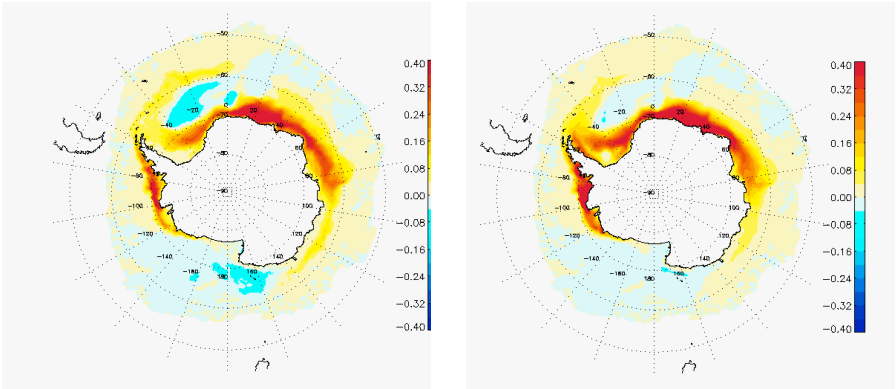

Figure 6: Differences in ice concentration (in %; (left panel) and thickness (in m; right panel) between ICE_SHEET experiment and REF experiment in mean 1993-2012 September.

Discussion

This short paper presents an intercomparison between the LIM2 and LIM3 sea ice models as available from the last NEMO release. For this first assessment we used LIM3 as it is available and did not perform any calibrations regarding the use at ¼° resolution. The model results are generally similar, with some notable differences in terms of summer ice extent and horizontal sea ice thickness distribution. It is too early to diagnose the origin of the differences between the models. LIM3 gives encouraging results especially regarding winter ice thickness and summer ice extent, confirming previous studies (Vancoppenolle et al., 2009a; Massonnet et al., 2011). As sea ice strongly responds to the atmospheric surface boundary conditions in forced configurations, more work is needed (i) to improve the subjective assessment presented here, and (ii) to calibrate LIM3 and the atmospheric forcing parameters to improve the ice reconstruction. A dedicated methodology to properly evaluate the ice thickness distribution simulated by a multi category sea ice model is ongoing. Further work is certainly also needed to adapt the interfaces with the ocean underneath and the atmosphere above in order to take into account the heterogeneous surface in a grid-mesh. Last, LIM3 is planned to be tested in a Mercator 1/12° horizontal resolution configuration to evaluate its potential implementation in the future global operational system of the Copernicus Marine Service.
By combining numerous techniques (altimetry, gravimetry, models, etc …) to estimate the surface mass balance of polar ice caps (see for example Shepherd et al., 2012), it is now feasible to build a comprehensive freshwater flux from polar ice cap melt adapted for OGCMs in the altimeter era. The present work is a first step towards this goal and work is underway to further improve the representation of the continental ice sheet forcing on the oceanic circulation: the seasonal cycle of the flux may be revised by considering gravimetry estimates and interannual variability of liquid and solid contribution (Enderlin et al., 2014). This interannual forcing may be used to feed the iceberg model recently implemented in the NEMO model. The next step on the sensitivities experiment methodology will be to take into account a climatological ice cap forcing to estimate the increase of the melting over the past two decades. Given the important changes experienced by the polar ice caps, there is an urgent need for near real time monitoring of the polar ice caps for operational applications.

Acknowledgments

This work has received funding from the European Community's Seventh Framework Programme FP7/2007–2013 under grant agreement no. 218812 (MyOcean). Special thanks to our collaborators of the NEMO group.

References

C. M. Bitz, C.M. and W. H. Lipscomb W.H., 1999: An Energy-Conserving Thermodynamic Model of Sea Ice, J. of Geophys. Res., 104, 15,669-16,677.

Bouillon, S., Fichefet T., Legat, V. and Madec G. 2013: The elastic–viscous–plastic method revisited, Ocean Modelling, 71, 2-12.

Church, J.A. and co-authors, 2013: Sea Level Change. In: Climate Change 2013: The Physical Science Basis. Contribution of Working Group I to the Fifth Assessment Report of the Intergovernmental Panel on Climate Change. Cambridge University Press, Cambridge, United Kingdom and New York, NY, USA.

Comiso, J.C. 2000, updated 2014. Bootstrap Sea Ice Concentrations from Nimbus-7 SMMR and DMSP SSM/I-SSMIS. Version 2.. Boulder, Colorado USA: NASA DAAC at the National Snow and Ice Data.

Dai, A. and Trenberth, K.E. 2002, Estimates of freshwater discharge from continents: latitudinal and seasonal variations, J. Hydrometeorol., 3(6), 660-687.

Dee, D.P. and co-authors, 2011: The ERA-Interim reanalysis: configuration and performance of the data assimilation system. Q. J. R. Meteorol. Soc. 137: 553 – 597. DOI:10.1002/qj.82

Enderlin, E.M., Howat, I.M., Jeong, S., Noh, M.-J., van Angelen, J.H. and van den Broeke M.R. 2014: An improved mass budget for the Greenland ice sheet, Geophys. Res. Lett., 41, 866–872, doi:10.1002/2013GL059010.

EUMETSAT OSI SAF Global Reprocessed Sea Ice Concentration dataset v1.1, Product User Manual v1.3, October 2011, SAF/OSI/CDOP/met.no/TEC/MA/138.

Ezraty, R., Girard-Ardhuin, F., Piolle, J.-F., Kaleschke, L. and Heygster, G. 2007, Arctic and Antarctic sea ice concentration and Arctic sea ice drift estimated from Special Sensor Microwave data, User's Manual, Version 2.1, CERSAT.

Fichefet T. and Morales Maqueda, M.A. 1997, Sensitivity of a global sea ice model to the treatment of ice thermodynamics and dynamics, J. of Geophys. Res., 102, 12609–12646.

Hibler, W. D., 1979: A Dynamic Thermodynamic Sea Ice Model, J. Phys.Oceanogr., 9, 815–846.

Jakobson, E., Vihma, T., Palo, T., Jakobson, L., Keernik, H. and Jaagus, J. 2012, Validation of atmospheric reanalyses over the central Arctic Ocean, Geophys. Res. Lett., 39(L10802), doi:10.1029/2012GL051591.

Kern, S., Khvorostovsky, K., Skourup, H., Rinne, E., Parsakhoo, Z. S., Djepa, V., Wadhams, P., and Sandven, S.: The impact of snow depth, snow density and ice density on sea ice thickness retrieval from satellite radar altimetry: results from the ESA-CCI Sea Ice ECV Project Round Robin Exercise, The Cryosphere, 9, 37-52, doi:10.5194/tc-9-37-2015, 2015.

Kwok, R., Cunningham, G.F., Wensnahan, M., Rigor, I., Zwally, H.J. and Yi, D. 2009, Thinning and volume loss of the Arctic Ocean sea ice cover:2003-2008, J. Geoph. Res., 114-C07005, doi:10.1029/2009JC005312.

Large, W. and Yeager, S.: Diurnal to decadal global forcing for ocean sea ice models: the data set and fluxes climatologies, Rep. NCAR/TN-460+STR, National Center for Atmospheric Research, Boulder, Colorado, 2004.

Lellouche, J.-M., Le Galloudec, O., Drevillon, M., Regnier, C., Greiner, E., Garric, G., Ferry, N., Desportes, C., Testut, C.-E., Bricaud, C., Bourdalle-Badie, R., Tranchant, B., Benkiran, M., Drillet, Y., Daudin, A. and De Nicola, C. 2013, Evaluation of global monitoring and forecasting systems at Mercator Ocean, Ocean Sci., 9, 57-81; doi:10.5194/os-9-57-2013.

Levitus, S. and coauthors, 1998: Introduction. Vol. 1, World Ocean Database 1998. NOAA Atlas NESDIS18, NOAA/NESDIS, U.S. Dept. of Commerce, Washington, D.C.

Lüpkes, C., Vihma, T., Jakobson, E., Konig-Langlo, G. and Tetzlaff, A. 2010: Meteorological observations from ship cruises during summer to the central Arctic: A comparison with reanalysis data, Geophys. Res. Lett., 37(L09810), doi:10.1029/2010GL042724.

Madec, G. 2008: NEMO ocean engine, Note du Pole de modelisation, Institut Pierre-Simon Laplace , France, 27, 1288–1619.

Marsh, R., Ivchenko, V.O., Skliris, N., Alderson, S. Bigg, G.R., Madec, G., Blaker, A. and Aksenov, Y. 2014, NEMO-ICB (v1.0): interactive icebergs in the NEMO ocean model globally configured at coarse and eddy-permitting resolution., Geosci. Model Dev. Discuss., 7, 5661-5698

F. Massonnet, T. Fichefet, H. Goosse, M. Vancoppenolle, P. Mathiot, and C. Konig Beatty, 2011: On the influence of model physics on simulations of Arctic and Antarctic sea ice, The Cryosphere, 5, 687–699.Product User Guide, version 2.0, Sea Ice Climate Change Initiative Phase 1, European Space Agency

Ramillien, G., Lombard, A., Cazenave, A., Ivins, E.R., Llubes, M., Remy, F. and Biancale R. 2006:, Interannual variations of the mass balance of the Antarctica and Greenland ice sheets from GRACE, Global Planet.Change, 53, 198– 208, doi:10.1016/j.gloplacha.2006.06.003.

Rignot E., Box, J.E., Burgess, A. and E. Hanna, E. 2008: Mass balance of the Greenland ice sheet from 1958 to 2007. Geophys. Res. Lett..

Rousset, C., Vancoppenolle, M., Madec, G., Fichefet, T., Benshila, R., Chanut, J., Flavoni, S., Levy, C. and Masson S.: The Louvain-La-Neuve sea-ice model LIM3.5: Global and regional capabilities. Geoscientific Model Development, NEMO special issue, in prep.

Semtner, A.J. 1976: A model for the thermodynamic growth of sea ice in numerical investigations of climate, J. Phys. Oceanography. 6, 379-389.

Shepherd, A. et al. 2012: A reconciled estimate of ice-sheet mass balance, Science, 338(6111), 1183–1189, doi:10.1126/science.1228102.

Silva, T.A.M , Bigg, G.R. and Nicholls, K.W. 2006: Contribution of giant icebergs to the southern ocean freshwater flux. Journal of geophysical research, vol. 111.

Thorndike, A. S., D. S. Rothrock, G. A. Maykut and R. Colony, 1975: The thickness distribution of sea ice. J. Geophys. Res., 80, 4501-4513.

Timmerman, R., Goosse, H., Madec, G., Fichefet, T., Ethe, C.,and Duliere, V., 2005: On the representation of high latitude processes in the ORCA-LIM global coupled sea ice-ocean model, Ocean Model., 8, 175–201.

Tournadre, J., Whitmer, K. and Girard-Ardhuin, F. 2008: Iceberg detection in open water by altimeter waveform analysis, J. Geophys. Res., 113, C08040, doi:10.1029/2007JC004587.

Vancoppenolle, M., Fichefet, T., Bitz, C.M. 2006. Modeling the salinity profile of undeformed Arctic sea ice. Geophysical Research Letters 33, L21501. doi:10.1029/2006GL028342.

Vancoppenolle, M., Bitz, C.M., Fichefet, T. 2007: Summer landfast sea ice desalination at Point Barrow, Alaska: model and observations. Journal of Geophysical Research 112, C04022. doi:10.1029/2006JC003493.

Vancoppenolle, M., Fichefet, T., and Goosse, H., 2009a: Simulating the mass balance and salinity of Arctic and Antarctic sea ice, 2. Im-portance of salinity variations, Ocean Model., 27, 54–69.

Vancoppenolle, M., Fichefet, T., Goosse, H., Bouillon, S., Madec, G. and Morales Maqueda, M.A. 2009b: Simulating the mass balance and salinity of Arctic and Antarctic sea ice. 1. Model description and validation. Ocean Modelling 27 (1), 33-53.

PARAMETERIZATION OF DRAG COEFFICIENTS OVER POLAR SEA ICE FOR CLIMATE MODELS

By Christof Lüpkes[1] and Vladimir M. Gryanik[1,2]

[1] Alfred-Wegener-Institut Helmoltz-Zentrum für Polar- und Meeresforschung, Bremerhaven, Germany
[2] A.M. Obukhov Institute of Atmospheric Physics, Russian Academy of Sciences, Moscow, Russia.

Abstract

A parameterization of drag coefficients has been developed in recent years that accounts for the impact of edges at ice floes, leads, and melt ponds on momentum transport. Melt ponds are a common feature in the inner Arctic during summer while drifting ice floes and their edges influence the surface roughness especially in the marginal sea ice zones during all seasons. Governing parameters in the parameterization that can be easily applied to climate models are the sea ice concentration and aspect ratio h/D where h is the ice freeboard and D is the characteristic length of floes and ponds/leads. When these parameters are not available from a sea ice model, the aspect ratios can also be parameterized as a function of the sea ice concentration so that the new schemes can also be used in stand-alone atmospheric models using observed sea ice concentration. The parameterization is evaluated for idealized meteorological forcing and prescribed sea ice and melt pond concentration in the Siberian Arctic and in parts of the Central Arctic. The required sea ice data are available from remote sensing. The distributions of drag coefficients obtained from traditional parameterizations and from the new one show large differences in this test scenario especially in the region south of 80°N.

Introduction

Neutral drag coefficients observed over polar sea ice show a large variability with values roughly between 0.5×10^{-3} and 4×10^{-3} (Anderson, R.J., 1987; Andreas et al., 1984; Overland, 1985; Fairall and Markson, 1987; Guest and Davidson, 1987; Hartmann et al., 1994; Kottmeier et al., 1994; Mai et al., 1996; Garbrecht et al., 2002; Schröder et al., 2003). This variability is caused by the inhomogeneous sea ice surface topography which is a result of convergent and divergent sea ice drift causing the formation of ridges, small floes and leads. Also melting processes influence the sea ice topography due to the formation of melt ponds and related edges.

There have been many attempts in the past to parameterize the sea ice roughness with various concepts. The focus here is on schemes that distinguish between skin drag, related to the relatively smooth surface of level ice, and form drag caused by the edges of the ridges, floes and melt ponds. Such schemes have been developed especially for the marginal sea ice zones (MIZ) where the variability of roughness is mainly caused by the inhomogeneous distribution of floe edges (Hanssen-Bauer and Gjessing, 1988; Mai et al., 1996; Stössel and Claussen,1993; Steiner (2001), Birnbaum and Lüpkes, 2002; Lüpkes and Birnbaum, 2005). Since the number density of edges is connected with the sea ice concentration A, the latter can be used as a dominating parameter for the drag coefficients.

The dependence on A has been shown by Andreas et al. (2010) on the basis of measured drag coefficients also for the inner Arctic during summer when leads and melt ponds have formed. They proposed a quadratic dependence of the neutral 10 m drag coefficient C_{dn10} on A which resulted from a fit to drag coefficients derived from in-situ turbulence data over the Beaufort Sea and the marginal sea ice zone. In typical conditions results of this fit do not differ much from the results of the more complex parameterizations mentioned above. Thus this approach can be considered as a progress and it shows furthermore that the A related parameterization of C_{dn10} is possible in a much larger region than the MIZ. The drawback is, however, that this approach does not allow the adjustment of the drag coefficients to variable sea ice topography and does not allow coupling with the usual wind speed dependent parameterizations of the drag coefficients over water, which should be possible at least for small sea ice cover.

A further step followed by Lüpkes et al. (2012) (LU12). They showed that the quadratic fit proposed by Andreas et al. (2010) can be obtained as a special case of the above mentioned more general and physically based drag partitioning concept, when this is extended e.g. to include also inner Arctic conditions and when certain simplifying assumptions are made. The LU12 parameterization will be explained and discussed in section 2. It includes the dependence of drag coefficients on sea ice topography parameters and allows the formulation of the required neutral drag coefficients for sea ice models. Lüpkes and Gryanik (2015) included later the dependence of drag coefficients on stability which is explained here in its lowest level of complexity.

In sections 3 and 4, we show practical consequences of the new parameterization by comparing its results with those of a typical parameterization used currently in climate models.

Form drag dependent parameterization of momentum fluxes

The concept of drag partitioning together with flux averaging results in the effective neutral drag coefficients over a surface consisting of water and ice of concentration A so that:

$$C_{dn10} = C_{dn10,w}\,(1-A) + C_{dn10,i}\;A + C_{dn10,f}\;, \qquad (1)$$

where $C_{dn10,w}$ and $C_{dn10,i}$ are the neutral skin drag coefficients over water and ice at 10 m height and $C_{dn10,f}$ is the form drag coefficient for neutral stratification. Applying some algebra, LU12 proved that this approach (1) is equivalent with the Andreas et al. (2010) fit when fixed values are prescribed for $C_{dn10,w}$ and $C_{dn10,i}$ and when $C_{dn10,f}$ is proportional to A (1-A). Since the latter cannot be expected in general, LU12 investigated also whether this kind of A dependence exists in special conditions. To that aim, they derived first $C_{dn10,f}$ by calculating the dynamic pressure against floe edges similarly as proposed already by Hanssen-Bauer and Gjessing (1988) and by Arya (1975) (but now in 3D formulation and using less restrictive assumptions). They arrived finally at:

$$C_{dn10,f} = (c_e/2)\;[\,\ln(h_f / z_{0w}) / \ln(10/e\,z_{0w})\,]^2\;(S_c)^2\;(h_f / D_i)\;A \qquad \text{(MIZ)} \qquad (2)$$

$$C_{dn10,f} = (c_e/2)\;[\,\ln(h_p / z_{0w}) / \ln(10/e\,z_{0w})\,]^2\;(S_c)^2\;(h_p / D_w)\,(1-A)\,, \qquad \text{(inner Arctic)} \qquad (3)$$

where e = 2.718 is the Eulerian constant and all units of parameters are in meters. z_{0w} and z_{0i} are the skin drag related roughness lengths over open water and sea ice, h_f is the sea ice freeboard of drifting floes in the MIZ, h_p is the freeboard of ice related to the water surface in melt ponds/leads. D_i and D_w are the diameters of floes and ponds/leads and S_c are functions accounting for the sheltering of wind by ice floes. They can be set either to 1 or can be parameterized in terms of A in the simplest cases (see LU12). c_e is a constant that contains the coefficient of resistance of an individual roughness element, and that accounts for the floe and pond geometry (its deviation from a circular shape). For simplicity, we use the same letter for drag coefficients in the MIZ and inner Arctic and do the same for the sheltering functions although they differ from each other in general.

It is remarkable that the dependence of the drag coefficients in equations (2) and (3) on the sea ice concentration is different in both sea ice regimes. The reason is that there are differences between both morphologies. For example, sea ice floes appear to be disconnected in the MIZ case (at least for moderate values of the sea ice concentration) while the ice areas surrounding ponds are approximately connected. A further difference is that edges have a concave shape in the case of melt ponds and a convex one in the case of floes in the MIZ with regard to the upstream flow. Hence the formulae for the inner Arctic and MIZ differ in this general form from each other and differ a lot also from the AN10 quadratic fit that is proposed for both regions.

In the form (2) and (3) the parameterization can be applied to ocean or atmosphere models when they are coupled with a sea ice model providing the topography parameters. While these models provide h_f and h_p which are connected with the sea ice thickness, it is more difficult to obtain D_i and D_w. This problem has been solved by LU12 by showing that the latter two parameters, and in the most simplified level of the parameterization also h_f and h_p, can be parameterized as a function of the sea ice concentration. To that aim they used satellite observations of melt ponds (Fetterer et al., 2008) and aircraft observations of floe parameters over the MIZ from the campaigns REFLEX (Hartmann et al., 1994; Mai et al., 1996).

Inserting these parameterizations and using typical values for the roughness lengths, LU12 obtained the formulation:

$$C_{dn10,f} = C\;A\,(1-A)^{\beta} \qquad (4)$$

It is valid for both MIZ and inner Arctic with ponds/leads but with different values of constants (MIZ: $C = 3.67\times10^{-3}$, $\beta = 1.4$; inner Arctic: $C = 2.23\times10^{-3}$, $\beta = 1.1$). The scatter of observed topography parameters around the parameterized curves (see LU12) suggests that the parameters β and C should not be considered as fixed values. We expect that the possible ranges are large with $1.3\times10^{-3}<C<4.5\times10^{-3}$ and $0.3<\beta<1.8$ so that this range is allowed for sensitivity studies aiming at an improved understanding of the ice-air-ocean interaction processes.

The functional dependence on A which is required for the analogy to the Andreas et al. (2010) fit is approximately obtained by (4) using the given values for C and β for the inner Arctic, and it is exactly obtained for $\beta = 1$. It has to be stressed, however, that this equivalence is obtained only under restrictive assumptions ignoring, for example, that aspect ratios can vary also for fixed values of A, and also that in general, for example h_p and D_w depend in a more complex way on A than was assumed to obtain (4). For this reason, the parameterization (1) with (2) and (3) should be chosen when the topography parameters are available from sea ice models, and equation (1) with (4) is appropriate in stand-alone-atmosphere models. We will refer to the latter as the AWI parameterization in the following.

There is one further aspect of the parameterization that was considered by Lüpkes et al. (2013). This concerns the definition of A. In previous parameterizations melt ponds have never been considered as a source of roughness. Since this is different for equations (2), (3) and (4), A has to be redefined not as the sea surface related ice fraction A_{SSI} as usually done, but as the ice surface related fraction so that $A = A_{SSI} - A_p$ where A_p is the fraction of ponds on floes in a grid cell. The relevance of this change is explained in the next section.

Equations (1) with (4) give the effective drag coefficient for a grid cell with open water and sea ice. However, in models using flux averaging, the fluxes have to be separated into a contribution over open water and another one over sea ice. The latter contribution is needed also in sea ice models. Form drag modifies the fluxes over ice only so that the effective drag coefficient over ice is obtained as:

$$C_{dn10,i,eff} = C_{dn10,i} + C_{dn10,f} / A \;. \qquad (5)$$

Since in (4) β is only slightly different from 1 in the inner Arctic, equation (5) shows that in this case $C_{dn10,i,eff,}$ which is needed to calculate the momentum flux per unit ice area, depends quasi linearly on A. We stress that this dependence holds only when the large simplifications described above are carried out. In general, however, the dependence is nonlinear and this holds also for the effective drag coefficient C_{dn10} over the mixture of ice and open water (equation (1) with (4)).

Results of neutral drag coefficients for different scenarios

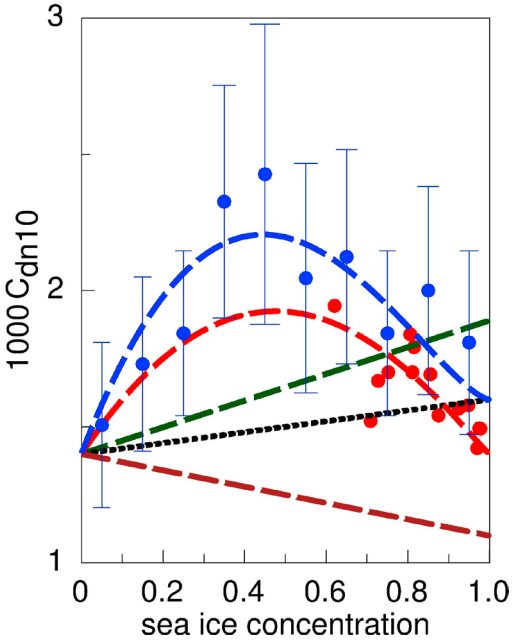

For simplicity, we discuss in the following only results obtained with the AWI parameterization (equation (1) with (4)) and compare them with results of parameterizations used for some state-of-the art climate models (ECHAM5/6, Roeckner et al., 2003; Giorgetta et al., 2012; CAM5, Neale et al., 2010) and for the momentum forcing of the ocean model MITgcm (Marshall et al., 1997). In these parameterizations only skin drag (equation 1 with $C_{dn10,f}$ = 0) is considered. We start with Figure 1 showing observations versus results of the parameterizations. Observed data result from aircraft observations (REFLEX) mentioned above and from the SHEBA campaign (ASFG tower) as analyzed by Andreas et al. (2010). Prior to 2013 effective drag coefficients used in GCMs depended linearly on A and form drag was included implicitly in the parameterizations by adjusting $C_{dn10,i}$ to high values. This contrasts with the results of the AWI parameterization and with measurements showing a nonlinear dependence on A.

Figure 1: Neutral drag coefficients at 10 m height obtained from measurements (circles) and form parameterizations (lines). Red circles: Measurements over the Beaufort Sea (Andreas et al., 2010) and over the Fram Strait marginal sea ice zone (Hartmann et al. 1991, Mai et al., 1996). Red line: AWI parameterization (equation 1 with 4) for summer sea ice with ponds and leads. Blue line: AWI parameterization for MIZ conditions. Brown line: forcing suggested by Nguyen et al. (2011) for the MITgcm. Black dotted line: CAM5 parameterization. Green line: current ECHAM6 parameterization (see also text).

As a first test, Lüpkes et al. (2013) used the AWI parameterization to calculate the distribution of drag coefficients over the whole Arctic Ocean for prescribed homogeneous wind speed and compared the results with those from the parameterizations used in the GCMs considered above. Large differences were found for the general Arctic-wide distribution of the drag coefficients. Compared with the new parameterization the traditional parameterizations underestimated the drag coefficients in the regions with large melt pond cover and lead fraction (e.g. in the Beaufort Sea region).

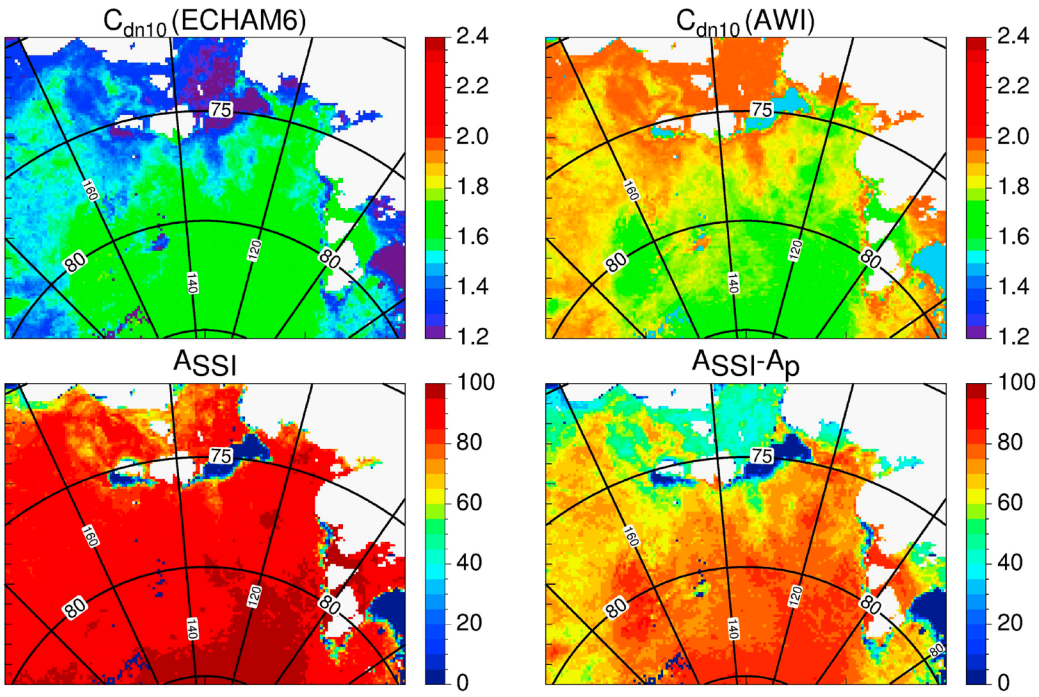

Figure 2: Neutral drag coefficients at 10 m height (Cdn10) obtained with the ECHAM6 parameterization and with the AWI parameterization (equation 1 with 4) over the Laptev Sea/East Siberian Sea and parts of the central Arctic. ASSI is the sea ice concentration as used in current climate models e.g. in ECHAM6 (no melt ponds considered), ASSI – Ap = A is the sea ice concentration used in the AWI parameterization that accounts for melt ponds. Ap is the melt pond fraction. Sea ice and melt pond fraction represent a 1 week average in June 2004 and are based on remote sensing (see text).

We consider in Figure 2 results of a similar study, but now only for a selected region in the Eastern Arctic (Siberian Sea, Laptev Sea, part of Central Arctic). Neutral drag coefficients are shown which were obtained with the ECHAM5/6 parameterization and with the AWI parameterization (equation 1 with 4 using parameter values for the inner Arctic). Sea ice and melt pond fraction were provided from the *Integrated Climate Data Center (ICDC), CliSAP/KlimaCampus, University of Hamburg, Germany* (http://icdc.zmaw.de) (see also Rösel et al., 2012). It can be seen that the largest differences between both parameterizations occur in the region south of 80°N. There, the large melt pond cover causes an increase of form drag and thus increases the drag coefficients obtained with the AWI parameterization. On the contrary, drag coefficients obtained with the ECHAM parameterization decrease in this region relative to the values north of 80°N since only skin drag is considered and due to the differences in the ice concentration variables A_{SSI} used in the traditional parameterization and A_{SSI}-A_p used in the AWI parameterization.

Generalized AWI parameterization for stability dependent drag coefficients

Sea ice covered regions are often characterized by strongly stable stratification of the atmospheric boundary layer. Furthermore, especially during winter, large differences can occur between the stratification over ice and open water so that the stability dependence of drag coefficients has to be taken into account in the parameterization. For this reason Lüpkes and Gryanik (2015) formulated a parameterization of the form drag coefficient which is similar to equations (2) and (3) but accounts for the fetch and stability dependence of wind on the upstream side of floe, melt pond, and lead edges. In its most simplified level, the stability dependent form drag coefficient at 10 m height is given by:

$$C_{d10,f} = C_{dn10,f} [(1-A) f_{m,w} + A f_{m,i}] \quad , \qquad (6)$$

where $f_{m,w}$ and $f_{m,i}$ are stability correction functions over open water (w) and ice (i), formulated in terms of Monin-Obukhov theory or applying the Louis (1979) concept as a function of the bulk Richardson numbers over ice and open water. In this level $C_{dn10,f}$ is again given by equation (4) but with slightly modified values of the constant C (for summer: C = 2.20, for the MIZ: C = 3.54).

Roughness elements like floe edges increase the mechanical turbulence which also influences the heat flux. Thus a parameterization corresponding to (4) and (6) was derived by Lüpkes and Gryanik (2015) also for the heat transfer coefficient which is not discussed further here, but which should be used together with the stability dependent parameterization of the form drag.

To get an impression of the stability impact we show as a test of the parameterization results in Figures 3 and 4 for C_{d10} (equation 1 with 4 and 6) for idealized cases of warm air advection. In one case, the air is prescribed to be warmer than the ice and water surface (Figure 3), in a second case, the air temperature is still warmer than the ice surface, but colder than the water surface (Figure 4). For the test, we prescribed in the whole area constant values for the wind speed and for the air and surface temperatures of ice and water. The used values (see figure caption) can occur during summer over large parts of the Arctic. The stability functions $f_{m,w}$ and $f_{m,i}$ have been calculated using the Louis (1979) concept as in ECHAM6 (Giorgetta et al., 2012) and in the coupled model ECHAM6-FESOM (Sidorenko et al., 2014). A comparison of the drag coefficients with Figure 2 for neutral conditions shows the strong impact of stability although we considered cases with only small deviations from neutral stratification. In the region with large melt pond cover (south of 80°N) drag coefficients obtained with the AWI parameterization decrease slightly in the stable case, but they increase strongly in the unstable case. Obviously, the new parameterization reacts stronger than the ECHAM6 parameterization on small changes in stability which leads to the asymmetric response in the shown cases. As for neutral conditions, differences between the ECHAM6 parameterization and the AWI parameterization are also largest south of 80°N. Lüpkes et al. (2015) show furthermore that the sea ice concentration, for which the drag coefficients attain their maximum values, depends on the stability and that this dependence differs in the new and traditional parameterizations as can be seen also in the present figures. Thus the new schemes might help to better understand momentum exchange between air and sea ice and related effects in a changing climate with changing temperature conditions and sea ice concentration.

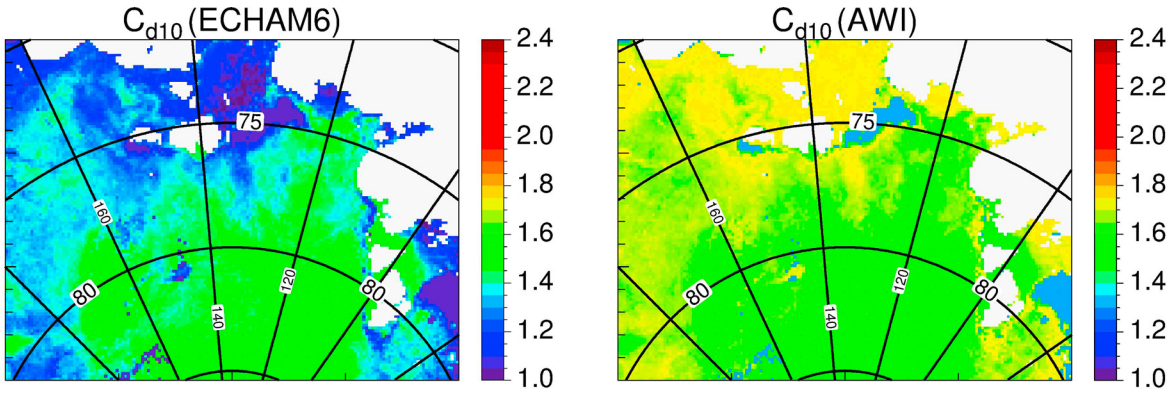

Figure 3: Drag coefficients at 10 m height (Cd10) obtained with the ECHAM6 parameterization and the AWI parameterization (equation 1 with 4 and 6). The same sea ice and melt pond data are used as in Figure 2 but the results represent a case with weak warm air advection and thus stable stratification over ice and water. Prescribed surface temperatures are 272.8 K over ice and 272.5 K over water. Air temperature is set to 273.5 K. Wind speed is 5 m/s. Ice concentration is prescribed as in Figure 2.

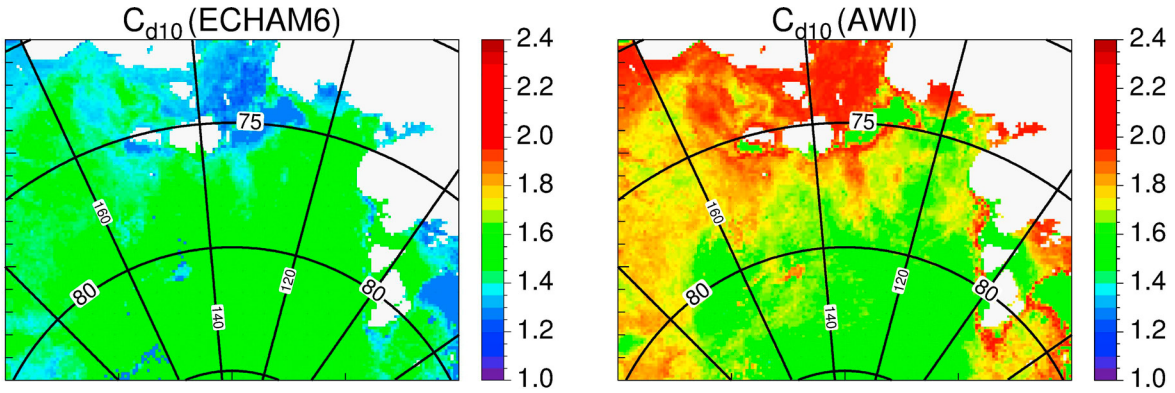

Figure 4: Same as Figure 3, but for a case with stable stratification over ice and unstable stratification over water. Surface temperature over water is set to 271.5 K and over ice to 268 K. Air temperature is 269 K. Ice concentration is prescribed as in Figure 2.

Conclusions

The interaction between atmosphere, sea ice, and ocean depends strongly on the transfer coefficients for momentum and heat. Observations show that in regions with fractional sea ice cover the neutral transfer coefficients for momentum are closely linked with the sea ice concentration A and that they depend nonlinearly on A. Parameterizations of the momentum transfer coefficients reproduce the observed nonlinearity when a concept is used that distinguishes between skin drag over level ice and open water and form drag caused by the edges of floes, melt ponds and leads. A parameterization of the drag coefficients and their stability dependence by Lüpkes et al. (2012) and Lüpkes and Gryanik (2015) is available for climate models in different complexity levels. The most complex level can be used when sea ice topography parameters are known from a sea ice model, the lowest level is appropriate for a stand-alone atmospheric model using sea ice concentration e.g. from reanalysis.

Results have shown that the new parameterization has a large impact on drag coefficients especially in regions with large melt pond and lead cover such as in the Beaufort Sea and Siberian Sea regions. This holds especially when the stabilities over ice and open water differ from each other since form drag is influenced by both stabilities due to the fetch dependence of the wind profiles. Beyond the simple test cases shown in Figures 2, 3, and 4 the parameterizations should be implemented in climate models to better understand their role for ice-atmosphere interaction processes.

The new parameterizations have been developed following the traditional line including the effect of sea ice pressure ridges in the skin drag coefficient over ice. A possible extension of our approach to include the effect of ridges in the form drag coefficient was suggested by Tsamados et al. (2014) and by Castellani et al (2014).

Acknowledgments

We thank E.L Andreas for providing measured drag coefficients from SHEBA, J. Hartmann for data from the marginal sea ice zones (REFLEX), and L. Kaleschke for sea ice and melt pond data. We further thank E.L Andreas, J. Hartmann, G. Birnbaum W. Dorn, D. Sein, and D. Sidorenko for helpful discussions. This work contributes to the project MiKlip funded by the German Federal Ministry of Education and Research (FKZ: 01LP1126A).

References

Anderson, R.J. 1987: Wind stress measurements over rough sea ice during the 1984 Marginal Ice Zone Experiment, J. Geophys. Res. 92(C7): 6933–6941.

Andreas, E.L, Horst, T.W., Grachev, A.A., Persson, P.O.G., Fairall, C.W., Guest, P.S. and Jordan, R.E. 2010: Parametrizing turbulent exchange over summer sea ice and the marginal ice zone, Q.J.R. Meteorol. Soc.138: 927–943.

Andreas, E.L,Tucker III, W.B. and Ackley S.F. 1984: Atmospheric boundary-layer modification, drag coefficient, and surface heat flux in the Antarctic marginal ice zone, J. Geophys. Res. 89(C1): 649-661.

Arya, S.P.S. 1975: A drag partitioning theory for determining the large-scale roughness parameter and wind stress on the Arctic pack ice, J. Geophys. Res. 80, No 24: 3447-3454.

Birnbaum, G., and Lüpkes, C. 2002: A new parametrization of surface drag in the marginal sea ice zone, Tellus, Ser. A 54(1): 107–123.

Castellani, G., Lüpkes, C. Hendricks, S. and Gerdes, R. 2014: Variability of Arctic sea-ice topography and its impact on the atmospheric surface drag, J. Geophys. Res. Oceans119, doi:10.1002/2013JC009712.

Fairall, C.W. and Markson R. 1987: Mesoscale variations in surface stress, heat fluxes, and drag coefficient in the marginal ice zone during the 1983 marginal ice zone experiment, J. Geophys. Res. 92: 6921-6932.

Fetterer, F., Wilds, S. and Sloan, J. 2008: Arctic sea ice melt pond statistics and maps, 1999–2001, http://nsidc.org/data/docs/noaa/g02159_ponds/index.html, Natl. Snow and Ice Data Cent., Boulder, Colo.

Garbrecht, T., Lüpkes, C., Hartmann, J. and Wolff, M. 2002: Atmospheric drag coefficients over sea ice-Validation of a parametrisation concept, Tellus A 54(2): 205-219.

Giorgetta, M.A., et al. 2012: The atmospheric general circulation model ECHAM6. Model description, Max Planck Inst. for Meteorol., Hamburg, Germany, 27 September 2012, 156 pp.

Guest, P. S. and Davidson, K.L. 1987: The effect of observed ice conditions on the drag coefficient in the summer East Greenland Sea marginal ice zone, J. Geophys. Res. 92(C7): 6943-6954.

Hanssen-Bauer, I. and Gjessing Y.T. 1988: Observations and model calculations of aerodynamic drag on sea ice in the Fram Strait, Tellus, Ser. A, 40: 151-161.

Hartmann, J., Kottmeier,C., Wamser, C. and E. Augstein 1994: Aircraft measured atmospheric momentum, heat and radiation fluxes over Arctic sea ice, in The Polar Oceans and Their Role in Shaping the Global Environment, Geophys. Monogr. Ser., vol. 85, edited by O. M. Johannessen, R. D. Muench, and J. E. Overland, AGU, Washington, D. C.: 443-454.

Kottmeier, C., Hartmann, J. Wamser, C., Bochert, A., Lüpkes, C., Freese, D. and Cohrs, W. 1994: Radiation and eddy flux experiment 1993 (REFLEX II), Rep. Polar Res. 133, 62 pp., Alfred Wegener Inst., Bremerhaven, Germany.

Louis, J. F. (1979), A parametric model of vertical eddy fluxes in the atmosphere, *Boundary Layer Meteorol.*, *17*, 187–202.

Lüpkes, C. and Gryanik, V.M. 2015: A stability dependent parametrization of transfer coefficients for momentum and heat over polar sea ice to be used in climate models, *J. Geophys. Res. Atmos.*, *120*, doi:10.1002/2014JD022418.

Lüpkes, C., Gryanik, V.M., Rösel, A., Birnbaum, G. and Kaleschke, L. 2013: Effect of sea ice morphology during Arctic summer on atmospheric drag coefficients used in climate models, Geophys. Res. Lett., 40: 446-451, doi:10.1002/grl.50081.

Lüpkes, C., Gryanik, V.M., Hartmann, J. and Andreas E.L 2012: A parametrization, based on sea ice morphology, of the neutral atmospheric drag coefficients for weather prediction and climate models, J. Geophys. Res., 117, D13112, doi:10.1029/2012JD017630.

Lüpkes, C. and Birnbaum, G. 2005: Surface drag in the Arctic marginal sea-ice zone: A comparison of different parameterisation concepts, Boundary Layer Meteorol. 117: 179-211.

Mai, S., Wamser, C. and Kottmeier, C. 1996: Geometric and aerodynamic roughness of sea ice, Boundary Layer Meteorol. 77: 233-248.

Marshall, J., Adcroft, A., Hill, C., Perelman, L. and Heisey C. 1997: A finite-volume, incompressible Navier–Stokes model for studies of the ocean on parallel computers, J. Geophys. Res., 102(C3): 5753-5766.

Neale, R.B., Gettelman, A., Park, S., Conley, A.J., Kinnison, D., Marsh, D., Smith, A.K., Vitt, F., Morrison, H., Cameron-Smith, P., Collins, W.D., Iacono, M.J., Easter, R.C., Liu, X. and Taylor, M.A. 2010: Description of the NCAR Community Atmospheric Model (CAM 5.0), NCAR technical note, NCAR/TN-486 + STR, 268 pp.

Nguyen T., Menemenlis, D. and Kwok, R. 2011: Arctic ice-ocean simulation with optimized model parameters: Approach and assessment, J. Geophys. Res., 116, C04025, doi:10.1029/2010JC006573.

Overland, J. E. 1985: Atmospheric boundary layer structure and drag coefficients over sea ice, *J. Geophys. Res.*, *90*, 9029–9049.

Roeckner, E., Bäuml, G., Bonaventura, L, Brokopf, R., Esch, M., Giorgetta, M., Hagemann, S., Kirchner, I., Kornblueh, L, Manzini, E., Rhodin, A., Schlese, U., Schulzweida, U. and Tompkins, A. 2003: The atmospheric general circulation model ECHAM5. Part 1. Model description, *MPI Rep., 349*, Max Planck Inst. for Meteorol., Hamburg, Germany.

Rösel, A., Kaleschke, L. and Birnbaum, G. 2012: Melt ponds on Arctic sea ice determined from MODIS satellite data using an artificial neural network, The Cryosphere, 6, doi:10.5194/tc-6-431-2012.

Schröder, D., Vihma, T., Kerber, A. and Brümmer, B. 2003: On the parametrisation of turbulent surface fluxes over heterogeneous sea ice surfaces, J. Geophys. Res., 108(C6), 3195, doi:10.1029/2002JC001385.

Sidorenko, D., Rackow, T., Jung, T., Semmler, T., Barbi, D., Danilov, S., Dethloff, K., Dorn, W., Fieg, K., Gößling, H.F., Handorf, D., Harig, S., Hiller, W., Juricke, S., Losch, M., Schröter, J., Sein, D. and Wang, Q. 2014: Towards multi-resolution global climate modeling with ECHAM6-FESOM. Part I: Model formulation and mean climate, *Clim. Dyn*, doi:10.1007/s00382-014-2290-6.

Steiner, N. 2001: Introduction of variable drag coefficients into sea-ice models, Ann. Glaciol., 33, 181-186.

Stössel, A. and Claussen, M. 1993: On the momentum forcing of a largescale sea-ice model, Clim. Dyn. 9: 71-80.

Tsamados, M., D. L. Feltham, D. Schröder, D. Flocco, S. L. Farrell, N. Kurtz, S. W. Laxon and S. Bacon 2014: Impact of variable atmospheric and oceanic form drag on simulations of Arctic sea ice, *J. Phys. Oceanogr.*, *44*, 1329–1353, doi:10.1175/JPO-D-13-0215.1.

A MAXWELL-ELASTO-BRITTLE RHEOLOGY FOR SEA ICE MODELING

By Véronique Dansereau[1], Jérôme Weiss[2], Pierre Saramito[3], Philippe Lattes[4] and Edmond Coche[5]

[1] LGGE, CNRS UMR 5183, Université de Grenoble, Grenoble, France
[2] ISTerre, CNRS UMR 5275, Université de Grenoble, Grenoble, France
[3] LJK, CNRS UMR 5224, Université de Grenoble, Grenoble, France
[4] TOTAL S.A. - DGEP/DEV/TEC/GEO, Paris, France
[5] TOTAL S.A. - DGEP, Paris, France

Abstract

A new dynamical model, which builds on the recent elasto-brittle (EB) rheology, is developed in the context of the operational modeling of sea ice conditions over the Arctic. The EB model is modified by adding a viscous relaxation term to the linear-elastic constitutive relationship together with an ''apparent'' viscosity that evolves according to the local thickness, concentration and damage of the ice, like its elastic modulus. The coupling between the level of damage and both mechanical parameters is such that within an undamaged ice cover, the viscosity is infinitely large and deformations are strictly elastic, while along highly damaged zones, such as opening leads, the elastic modulus vanishes and most of the stress is dissipated through permanent deformations. In this augmented EB model, named Maxwell-EB after the Maxwell rheology, the irreversible and recoverable deformations are solved for simultaneously, hence ice drift velocities are defined naturally. Early idealized simulations, without advection but in which the ice is allowed to damage and heal, show the model is able to reproduce the strong heterogeneity and intermittency and the anisotropy that characterize the deformation of sea ice.

Introduction

A proper representation of the mechanical behavior of sea ice is essential for making reliable predictions of ice conditions and drift, especially over the fine scales involved in operational modeling. In recent years, statistical analysis of available ice buoy drift and Radarsat Geophysical Processor System (RGPS) drift data have revealed the strong heterogeneity and intermittency of Arctic ice deformation (Marsan et al., 2004; Rampal et al., 2008), suggesting that the deformation of the pack is mostly accommodated by elastic interactions and brittle fracturing over a wide range of scales. Current operational modeling platforms (e.g., TOPAZ4 : Sakov et al., 2012, Canadian Global Ice Ocean Prediction System : Smith et al.. 2014) and coupled climate models, some with and some without data assimilation, are based on the same viscous-plastic (VP) rheological framework put forth in the late seventies (Hibler, 1977; 1979). Yet, this rheology is inconsistent with the observed elasto-brittle behavior of pack ice (Weiss et al., 2007) and recent studies have demonstrated that although it can represent with a certain level of accuracy the mean, global (> 100 km) sea ice drift, it effectively fails at reproducing the right amount and the characteristics of sea ice deformation, especially at small (regional, daily) scales (Girard et al., 2009).

Over the last few years, a new rheological framework named ''elasto-brittle" (EB) has been developed as an alternative to the VP rheology for continuum sea ice models, in which the ice cover is treated as a two-dimensional, isotropic, elastic, damageable material (Girard et al., 2011). The model combines:

- A linear elastic constitutive relationship for a continuum solid under plane stress,

$$\sigma = E\varepsilon(U), \qquad (1)$$

with $\boldsymbol{\sigma}$, the stress tensor, $\boldsymbol{\varepsilon}$, the strain tensor (in terms of the displacement, $\boldsymbol{U}$) and E, the elastic modulus of sea ice.

- A Mohr-Coulomb criterion for brittle failure, in agreement with in-situ stress measurements (Weiss et al., 2007),

$$\tau = \mu\sigma_N + C, \qquad (2)$$

With $\boldsymbol{\tau}$ and $\boldsymbol{\sigma_N}$, the shear and normal stresses, C, the cohesion, setting the resistance to pure shear and μ, the internal friction coefficient, set to the value of 0.7 commonly used for geo-materials and ice (Byerlee, 1978; Jaeger and Cook, 1979; Weiss and Schulson, 2009). In the model, a noise is introduced in the spatial distribution of the ice strength through the cohesion parameter C to represent the material's natural heterogeneity associated with structural defects at the sub-grid scale, such as thermal cracks, serving as stress concentrators. The randomly drawn values of C span estimates from in-situ stress measurements in Arctic sea ice (Weiss et al., 2007).

- A progressive isotropic damage mechanism for the elastic modulus representing fracturing and lead formation within the pack. By this process, *E* drops when the stress state locally exceeds the Coulomb failure envelope, resulting in local strain weakening or "damaging". Consistent with previous damage rheological models, the level of damage of the sea ice cover in the EB framework is represented by a non-dimensional, scalar parameter, *d*, evolving between 0 ("completely damaged") and 1 (undamaged pack) and interpreted as a measure of defects (crack) density (Kemeny and Cook, 1986). Because of the long-range interactions in the elastic medium, local drops in *E* associated with the damaging of model elements imply a stress redistribution that can in turn induce damage of neighboring elements. By this process, damage therefore propagates within the pack.

First implementations of this rheology into short (3-days), stand-alone realistic simulations of the Arctic ice pack forced with reanalysis winds and *without advection* showed the EB model is able to reproduce the strong localization and the anisotropy of damage and agrees very well with the deformation fields estimated from RGPS data (Girard et al., 2011). In the context of longer-term simulations of ice conditions, over which advective processes can no longer be neglected, a suitable dynamical ice model however needs to represent not only the small deformations associated with

the fracturing of the elastic ice pack, but also the larger, permanent deformations occurring once the pack is fragmented and undamaged plates move relative to each other along open leads, setting the overall drift pattern and velocity of the ice, ***u***. The goal of this work is to develop such a rheological framework allowing a passage between small and large deformations while retaining the capacity of the EB model to reproduce the observed anisotropy and scaling properties of sea ice.

The Maxwell-EB model

Estimating unambiguously the ice velocity field over days and longer time periods requires distinguishing between the elastic (reversible) and the permanent (irreversible) deformations occurring once the pack is damaged. This is an intrinsic limitation of the EB rheology, since the linear-elastic model solves for the total deformation $(\varepsilon_{total} = \varepsilon_E + \varepsilon_P)$ of the material only. If no further assumptions are made on the part of the stress that is dissipated through permanent deformations after the onset of damaging, the EB model can effectively be used between two limit cases:

1. The first assumes that all of the deformation is elastic. If a stress is applied to the EB material during a time Δt and then removed, its deformation is entirely recovered, even if damage has occurred and the elastic modulus is degraded (see figure 1, left panels). The material returns to its initial position, and the velocity is effectively zero. For an initially undamaged, uniform material (or isolated model grid element) with elastic modulus E^0, the loading and unloading paths are represented respectively by the thick black line and dashed purple line on the stress-strain diagram of figure 2.

2. The second case makes the assumption that all the deformation becomes permanent. In this limit, the material retains its new position when the stress is removed, with the unloading path represented by the blue dashed line on figure 2, and the velocity is trivially estimated from the displacement as $u = \varepsilon_P / \Delta t$.

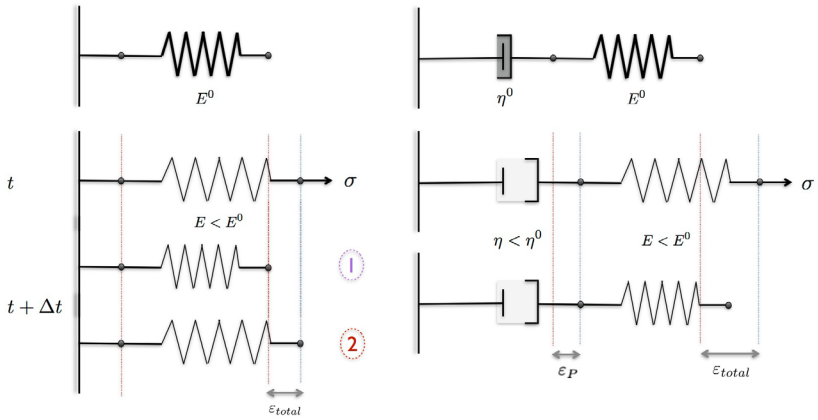

Figure 1: Schematic representations of the EB (left) and Maxwell-EB (right) models for a uniform material (or isolated model element) with initial, undamaged elastic modulus E^0 and viscosity η^0. At time t, an overcritical stress is applied on the system and is removed suddenly at time t+Δt. In the EB model, the spring deforms and weakens ($E < E^0$) when loaded. In the all-elastic deformation limit (1), it returns to its initial position when the system is unloaded. In the all-permanent deformation limit (2), it keeps its new position, and $\varepsilon_P = \varepsilon_{total}$. In the Maxwell-EB model, both the spring and dashpot deform under the applied stress such that $\varepsilon_{total} = \varepsilon_P + \varepsilon_E$, with a degradation of both E and η due to damaging. When the stress is removed, the spring returns to its initial position but the dashpot keeps its new position, resulting in a net permanent deformation, $\varepsilon_P \neq \varepsilon_{total}$.

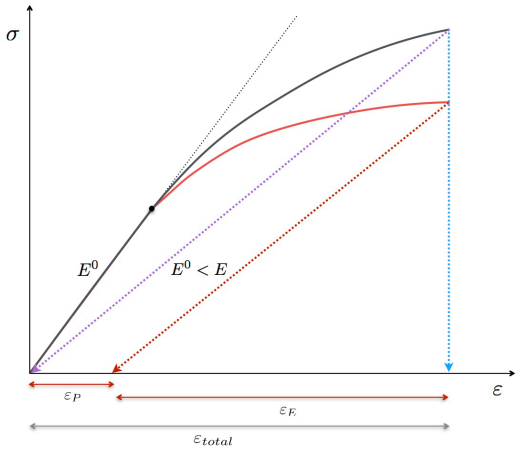

Figure 2: Stress-strain diagram for a linear-elastic (dotted curve), EB (plain black curve) and Maxwell-EB (red curve) material with initial uniform elastic modulus E^0. The black dot indicates the onset of damaging of the material. The purple and blue dashed lines represent the unloading paths for the EB material in the all-elastic and all-permanent deformation limits respectively. The red dashed curve represent the unloading path in the case of the Maxwell-EB model, with the red arrows partitioning the total deformation into the permanent and elastic contributions. It is important to note that the diagram is not to scale in the case of sea ice, in the sense that permanent deformations are usually much greater than elastic deformations.

In the case of sea ice, the second assumption might be justified by the fact that elastic deformations within an undamaged pack are small compared to the permanent deformations associated with the opening, closing, and shearing along leads. For instance, Bouillon et al. (unpublished) argued that there is a separation of 4 orders of magnitudes between the daily average deformation of a completely damaged ice pack in free drift mode and that of an undamaged, strictly elastic pack. However, in this limit, all of the stress is dissipated into permanent deformations at the end of each loading experiment, hence the *memory* of the stress associated with elastic deformations is erased after each simulated forcing increment (i.e., each model time step). Without carrying the history of previous stresses, the model cannot reproduce one important characteristic of the deformation which is its strong localization *in time*, or intermittency. In order to estimate adequate drift velocities while reproducing both the observed space and time scaling properties of sea ice deformation, a suitable rheological model must therefore have the capacity to distinguish between reversible and irreversible deformations.

In order to achieve this, we add a Newtonian fluid-like viscous damping term to the EB linear elastic constitutive equation, which then takes the form of the Maxwell rheology for continuum viscous-elastic materials:

$$\frac{1}{E}\frac{D\sigma}{Dt} + \frac{1}{\eta}\sigma = \dot{\varepsilon}(u), \qquad (3)$$

with $\dot{\varepsilon}(u)$ the strain rate. This Maxwell model is typically represented by a spring and a dashpot connected in series (see figure 1, right panels). When a stress is applied to the system, the resulting deformation is effectively split between two components: the instantaneous, reversible, deformation of the spring, $\boldsymbol{\varepsilon_E}$, and the permanent deformation of the dashpot, $\boldsymbol{\varepsilon_P}$, increasing linearly with time. For a given deformation applied to the Maxwell material $\boldsymbol{\varepsilon_{total}}$, the rate of dissipation of the associated stress through the permanent deformation of the dashpot is determined by the ratio, λ, of the viscosity of the dashpot, η, and the elastic modulus of the spring, *E*. As this characteristic relaxation time decreases, the capacity of the Maxwell material to propagate elastic constraints and retain the memory of reversible deformations also decreases. The introduction of a linear viscous term within damaged zones is justified by (i) the viscous-like rheology of highly fragmented (granular) media (Jop et al., 2006) and (ii) analogy between the mechanical behavior of sea ice and that of the lithosphere and the existence of "creeping" faults sliding aseismically within Earth's crust (Scholz, 2002).

The constitutive relationship in this modified EB model, named Maxwell-EB, differs from that of the standard Maxwell model in that the mechanical parameters *E, η* and *λ* are not constant but all coupled to the local level of damage of the material, *d*. The coupling is such that

- Undamaged areas of the ice cover undergo only small, strictly elastic deformations. These portions of the pack have an undamaged elastic modulus E^0 and an infinitely large apparent viscosity ($\eta^0 \rightarrow \infty$). In this limit, the viscous term (2nd term, LHS) in the Maxwell constitutive relationship (3) vanishes and a linear-elastic rheology is recovered.
- Over highly damaged areas of the pack, deformations are large as ice floes drift along open leads with much reduced friction. Both the elastic modulus and the apparent viscosity of the pack drop, resulting in larger instantaneous deformations that become irreversible more rapidly. Consequently, elastic interactions are inhibited and most of the stress applied to the ice cover dissipates into large, permanent deformations within a short relaxation time λ.

Different formulations can be used to couple *E, η* and *λ* in terms of *d* that respect the behavior described above. In the absence of physical evidence for a higher level of complexity, we chose the simplest parameterization and set $E = E^0 d$, $\eta = \eta^0 d^\alpha$ with $0<d \leq 1$ and α a constant parameter greater than one, introduced so that the relaxation time λ also decreases with increasing damage. As there is in theory no upper bound to this parameter, the appropriate value for α is determined through sensitivity tests. In a dynamic-thermodynamic model, E, η and λ would also be coupled to the concentration and thickness characteristics of the ice cover. In the following description of the uncoupled Maxwell-EB model, only the dependence on the level of damage is included.

In the Maxwell-EB framework, the level of damage of the ice cover evolves locally through two competing mechanisms: damaging and healing. At a given time, the decrease in *d* due to damaging is estimated as a function of the instantaneous distance of the local state of stress to the local damage criterion, $\boldsymbol{d_{crit}}$. The time, $\boldsymbol{t_d}$, associated with this change is deduced from the effective speed of propagation of elastic (shear) waves carrying the damage information within the ice cover, which is on the order of 500 m/s (Marsan et al., 2011). From current global climate to high resolution regional models, i.e., models with spatial resolution *Δx* ranging between 1 and 100 km, $\boldsymbol{t_d}$ varies between a few seconds and several minutes. The increase of d due to healing represents the re-consolidation and strengthening of the damaged ice pack due to the refreezing of open leads. This process is distinguished from pure thermodynamic growth in that it applies only where and when the ice has already been damaged. It therefore does not represent a net thickening of the ice cover and allows *d* to re-increase at *most* to its undamaged value of 1. The rate of healing is set by the characteristic time $\boldsymbol{t_h}$, corresponding to the time for a completely damaged element to regains its initial stiffness. In a coupled dynamic-thermodynamic model, $\boldsymbol{t_h}$ would depend on the difference between the temperature of the air above the ice and the freezing point of seawater below. In the present uncoupled model however, it is constant in both space and time and the rate of healing, set to $1/\boldsymbol{t_h}$, is therefore constant. Values on the order of 10^5 seconds are used for $\boldsymbol{t_h}$, based on studies on the refreezing within open leads (Petrich, 2007). Even though both processes act simultaneously on the level of damage, the orders of magnitude of difference between td and th imply that the mechanisms are intrinsically decoupled in time.

This new dynamic Maxwell-EB modeling framework for sea ice can therefore be summarized as a set of four equations:

- The momentum equation for sea ice

$$\frac{\partial u}{\partial t} + (u \cdot \nabla)u = F_{ext} + \nabla \cdot \sigma \qquad (4)$$

with the first term on the right hand side representing all external stresses on the ice and the last, the rheology term, the contribution from the mean internal stresses associated with the mechanical interactions between the ice floes,

The Maxwell constitutive relationship (3), with the elastic modulus and apparent viscosity of the ice entirely defined in terms of their initial, undamaged values and of the level of damage, *d*,

The equation of evolution for the level of damage, d, combining the rate of decrease due to damaging, set as a function of the local distance to the Mohr-Coulomb type damage criterion, and the rate of increase due to healing,

$$\frac{\partial d}{\partial t} + (u \cdot \nabla)d = f(d_{crit})\frac{1}{t_d}d + \frac{1}{t_h} \text{ with } 0 < d \leq 1. \qquad (5)$$

The advection equation for the cohesion field, C, which sets the local damage criterion,

$$\frac{\partial C}{\partial t} + (u \cdot \nabla)C = 0. \qquad (6)$$

Associated with the addition of the viscous relaxation term for the stress in the EB framework is the reformulation of the constitutive relationship in terms of the ice velocity, as opposed to the ice *displacement*, and the introduction of the time derivative of the stress tensor. The objective (Jaumann) derivative expends in three terms: an inertial term, an advection term, and rotation terms that arise because the Cauchy stress changes with rigid body rotation (rotation of the principal axes). Each of these contributions implies an increased level of numerical complexity. In developing the Maxwell-EB model, the approach taken is to introduce these terms separately and evaluate their contribution to the simulated dynamics. On the one

hand, introducing the inertial term first while neglecting advection (and rotation) allows retaining a Lagrangian scheme, similar to the EB model. If not employing adaptive remeshing methods, the model is then suitable for small-deformation simulations only. A large deformation, Eulerian, model on the other hand necessitates the inclusion of the non-linear advection term, with rotation terms becoming potentially important. In the following, first small-deformation experiments over domains with simplified geometries are analyzed in terms of the anisotropy, heterogeneity and intermittency of the simulated damage and deformation.

First simulation results: small-deformation experiments

When neglecting advection, the Maxwell-EB model reduces to three equations (3, 4, 5) for the ice velocity $\boldsymbol{u}$ (2 components), the state of stress $\boldsymbol{\sigma}$ (3 components), and the level of damage d. Time derivatives in the small-deformation model are approached with a Backward Euler scheme of order 1. A semi-implicit scheme is used to linearize the system, in which the momentum (4) and constitutive (3) equations are first solved simultaneously using the field of damage (i.e., the mechanical parameters E, η) at the previous time step. The level of damage is then updated using the newly estimated $\boldsymbol{u}$ and $\boldsymbol{\sigma}$. A fixed point algorithm iterates between these two computational steps, ensuring the convergence of the solution. The linear, time-discretized system of equations is solved using finite elements and variational methods within the C++ environment RHEOLEF (Saramito, 2013: http://cel.archives-ouvertes.fr/cel-00573970).

First simulations represent a two-dimensional, horizontal, rectangular plate of ice with height-to-width ratio of 2 under uniaxial compression (see figure 3, top left panel). The bottom edge of this sample is maintained fixed in the y-direction (with the position of the bottom left corner fixed in both directions). No confinement is applied on both lateral sides. The plate is compressed by prescribing Fext either as a small, constant increment of downward displacement (strain-controlled experiments) or force (stress-controlled experiments) on the upper boundary.

Here, two strain-driven uniaxial compression experiments are presented, the first with only the damaging mechanism operating and the second including both damaging and healing. The two simulations start with an undamaged plate with uniform elastic modulus E^0. The inverse of the viscosity η is set to zero when and where the ice is undamaged (d = 1) to represent the limit of $\boldsymbol{\eta 0} \rightarrow \infty$. The same cohesion field and unstructured mesh with triangular elements are used. The model is made completely dimensionless. The time step is set to unity, as the characteristic time for damage, $\boldsymbol{t_d}$, which ensures the highest resolution of damage propagation by the model. The characteristic time for healing is set to $\boldsymbol{t_h}$ = 10^5 seconds and a value of 4 is used for the exponent $\boldsymbol{\alpha}$.

Figure 3 shows the macroscopic stress as a function of the applied strain throughout the damage-only simulation (black line), with numbered panels showing the field of d at different stages of the loading experiment. The stress-strain relationship is initially linear as the undamaged material is strictly elastic. The blue line shows the number of overcritical elements as a function of the incremental strain. After the onset of damage (black dot), the material diverges from the linear-elastic behavior and experiences some strain-softening. In the early stage of damaging, damage is homogeneously scattered over the plate (d panel 1). Then as the number of overcritical elements increases, damage starts to localize (panel 2). A sharp increase in overcritical elements and subsequent large drop in macroscopic stress characterize the propagation of a distinct, oriented fault, or lead, throughout the sample (panels 3 and 4). Once this feature is formed, damaging stops. The macroscopic stress stabilizes at a low value, as the imposed strain is dissipated by creep along the lead. The shear and divergent strain rate fields, strongly correlated in space, indeed show that at this point deformation rates are orders of magnitude higher along the highly damaged than over the undamaged parts of the plate (bottom right panels).

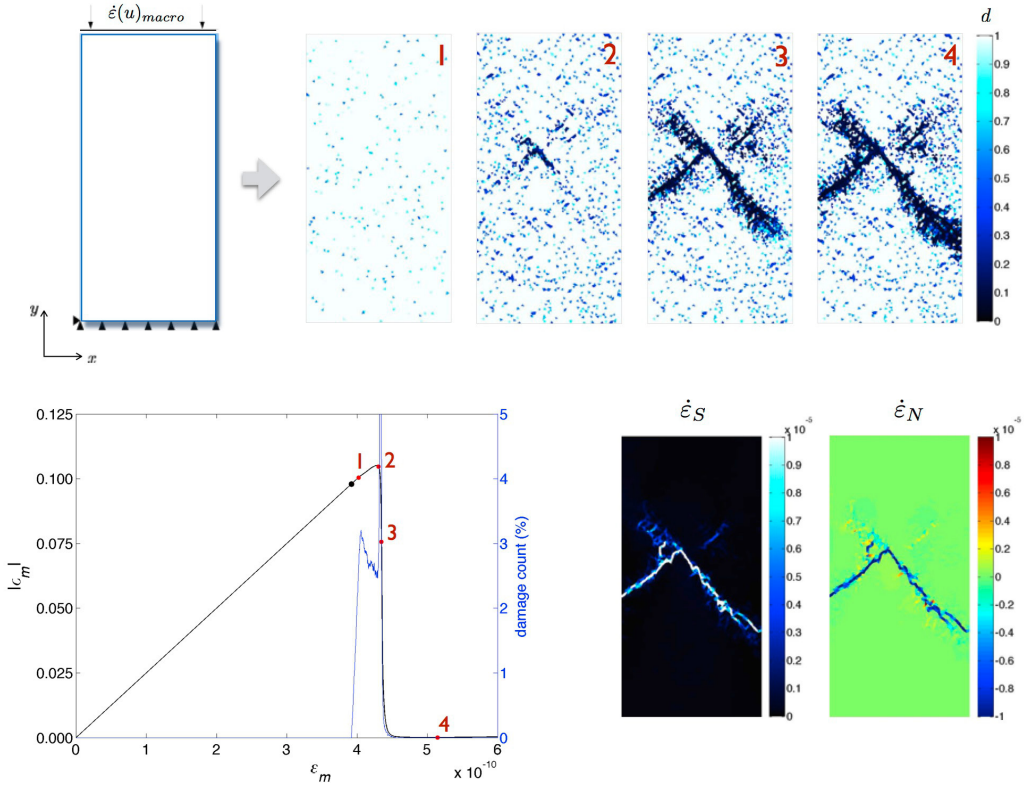

Figure 3: Results of the damaging-only uniaxial compression experiment. Top left panel: schematic representation of the boundary conditions and forcing imposed on the 2D simulated sample of ice. Bottom left panel: macroscopic stress as a function of the prescribed macroscopic strain (black curve) and corresponding percentage of overcritical model elements (blue curve). The black dot indicates the onset of damaging. Top right panels: level of damage at four stages of the experiments indicated on the stress-strain curve. Bottom right panels: shearing and divergence (positive) strain rates after the propagation of the main fault across the sample (stage 4).

When the compressive loading is maintained and the simulated material is also allowed to heal, a complex behavior emerges that is characterized by a succession of sharp stress drops associated with the localization of damage and propagation of faults and slower recovery periods during which the material regains some stiffness and stress buildups (see figure 4). These asymmetric and irregular cycles arise while the applied forcing is strictly uniform in time. Snapshots of the order of magnitude of the shearing deformation rate at different stages of the simulation (lower panels on figure 4) show that some cycles are associated with the re-activation of partially healed faults, while others are characterized by the formation of new features with different shapes and orientation, as observed in RGPS data (Kwok 2001). During stress-buildup phases, deformation increases everywhere over the sample. Stress drops abruptly when failure occurs and strain concentrates over the highly damaged areas, where it is orders of magnitude (≥3) higher than over undamaged areas. The experiment also reveals that in some instances, systems of fractures can remain activated for some time, in which case the macroscopic stress stabilizes (eg., panels 1 and 2), suggesting a balance between the rate of loading, the creeping and the rate of healing of the faults.

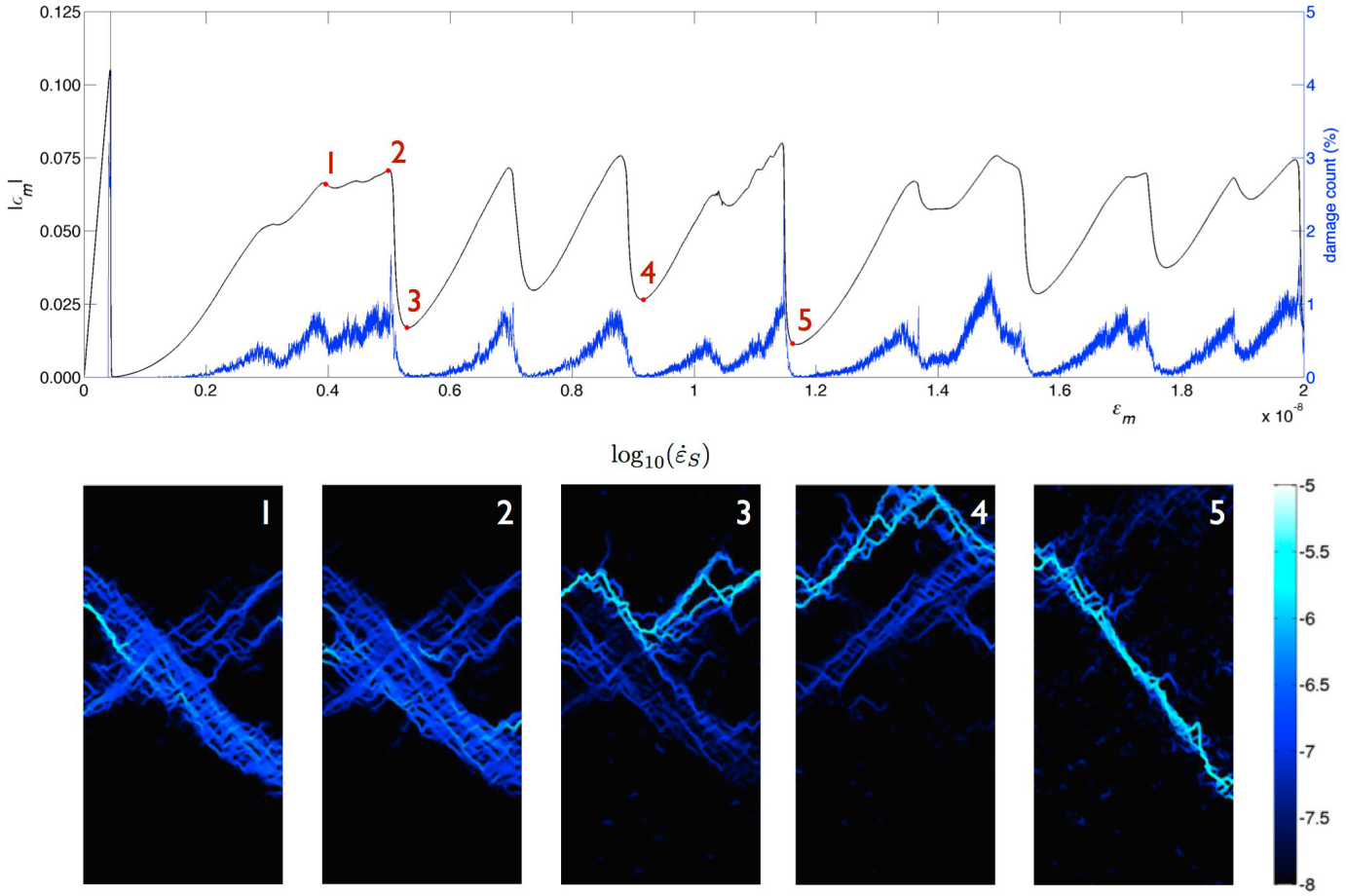

Figure 4: Results of the damaging and healing uniaxial compression experiment. Top panel: macroscopic stress versus macroscopic strain (black curve) and corresponding percentage of overcritical elements (blue curve). Bottom panels: Order of magnitude (logarithm in base 10) of the shearing deformation rate at the five stages indicated on the stress-strain plot.

In brief, these first experiments highlight important properties of the deformation simulated by the model:

1. the deformation is highly localized in space, i.e., heterogeneous (Marsan et al., 2004),
2. the deformation is strongly anisotropic, i.e. concentrates along linear kinematic features (Kwok 2001),
3. the deformation is localized in time, i.e, intermittent (Rampal et al., 2008).

As the applied strain increment is homogeneous in both space and time, these characteristics are not attributable to the external forcing but solely to the mechanics represented in the model.

Conclusion

First idealized experiments showed that the Maxwell-EB model is able to reproduce (1) the strong localization of deformation in both space and time, indicative of its heterogeneity and intermittency, (2) the natural emergence of the anisotropy of the deformation from an isotropic rheology (3) the asymmetry between successive periods of rapid damaging and slower recovery, (4) the persistence of activated leads (Coon et al., 2007) (5) the activation of new leads with different shapes and orientations, in agreement with the observed properties of the deformation of sea ice.

Sensitivity analyses and quantitative comparisons against Arctic buoy drift and RGPS deformation data are the next step in the development of the Maxwell-EB model. Such validation work necessitates carrying numerical experiments on realistic regional to global domains, over periods of days and longer. At these scales, deformations of the ice pack are large hence advection cannot be neglected. Unlike former, classical sea ice rheologies, the Maxwell-EB rheology effectively reproduces the very strong spatial gradients within the velocity, strain and stress fields of sea ice. This performance therefore requires the implementation of a robust advection scheme in order to limit diffusion and conserve the localization of the damage and deformation rates. The development of such an advection scheme is underway.

Acknowledgements

The financial support of TOTAL EP RECHERCHE DEVELOPPEMENT is gratefully acknowledged. V. Dansereau is supported by the Association National Recherche Technologie. She acknowledges support from the National Sciences and Engineering Research Council of Canada and the Fonds Québécois de la Recherche sur la Nature et les Technologies in the course of her Ph.D. A. Audibert-Hayet and K. Riska are thanked for valuable support and suggestions on this work.

References

Bouillon, S., J. Weiss, L. Girard, T. Fichevet, V. Legat and D. Amitrano: A further step towards the integration of the elasto-brittle rheology in sea ice models. Unpublished manuscript.

Byerlee, J., 1978: Friction of rocks. Pure and Applied Geophysics, 116(4-5), 615–626.

Coon, M. D., R. Kwok, G. Levy, M. Puis, H. Schreyer and D. Sulsky, 2007: Arctic Ice Dynamics Joint Experiment (AIDJEX) assumptions revisited and found inadequate. Journal of Geophysical Research, 112(C11S90), doi:10.1029/2005JC003393.

Girard, L., J. Weiss, J. M. Molines, B. Barnier, and S. Bouillon, 2009: Evaluation of high-resolution sea ice models on the basis of statistical and scaling properties of Arctic sea ice drift and deformation, Journal of Geophysical Research, 114, C08015, doi :10.1029/2008JC005182.

Girard, L., S. Bouillon, J. Weiss, D. Amitrano, T. Fichefet and V. Legat, 2011: A new modeling framework for sea-ice mechanics based on elasto-brittle rheology. Annals of Glaciology, 52(57), 123-132.

Hibler, W. D., III., 1977: A viscous sea ice law as a stochastic average of plasticity. Journal of Geophysical Research, 82, 3932 – 3938.

Hibler, W. D., III., 1979: A dynamic thermodynamic sea ice model. Journal of Physical Oceanogragphy, 9(7), 815–846.

Jaeger, J. C., and N. G. W. Cook, 1979: Fundamentals of rock mechanics. 593 pp.

Jop, P., Y. Forterre, and O. Pouliquen, 2006: A constitutive law for dense granular flows, Nature, 441, 727-730, doi:10.1038/nature04801.

Kenemy, J. and N. G. W. Cook, 1986: Effective moduli, Non-linear deformation and strength of a cracked elastic solid, International Journal of Rock Mechanics and Mining Sciences & Geomechanics Abstracts, 23(2), 107-118.

Kwok, R., 2001: Deformation of the arctic ocean sea ice cover between november 1996 and april 1997: a survey, Proceedings of the IUTAM Symposium on Scaling Laws in Ice Mechanics and Ice Dynamics, Fairbanks, Alaska, 315-322.

Marsan, D., H. Stern, R. Lindsay and J. Weiss, 2004: Scale dependence and localization of the deformation of arctic sea ice. Physical Review Letters, 93(178501).

Marsan D., J. Weiss, J.-P. Métaxian, J. Grangeon, P.-F. Roux, and J. Haapala, 2011: Low frequency bursts of horizontally-polarized waves in the Arctic sea-ice cover. Journal of Glaciology, 57(202), 231–237.

Petrich, C., P. Langhorne, and T. Haskell, 2007: Formation and structure of refrozen cracks in land-fast first-year sea ice, Journal of Geophysical Research, 112 (C4), C04,006.

Rampal, P., J. Weiss, D. Marsan, R. Lindsay, and H. Stern, 2008: Scaling properties of sea ice deformation from buoy dispersion analysis. Journal of Geophysical Research, 113(C03002), doi:10.1029/2007JC004143.

Sakov, P., F. Counillon, L. Bertino, K.A. Lisaeter, P. R. Oke and A. Korablev, 2012: TOPAZ4: an ocean-sea ice data assimilation system for the North Atlantic and Arctic. Ocean Sciences, 8, 633-656, doi:10.5194/os-8-633-2012.

Saramito, P., 2013: Efficient advanced scientific computing with Rheolef, CNRS-CCSD ed. http://cel.archives-ouvertes.fr/cel-00573970

Scholz, C.H., 2002: The Mechanics of Earthquakes and Faulting, Cambridge University Press, Cambridge, 471 pp.

Smith G. C., F. Roy, M. Rezka, M. Surcel, D. Colan, Z. He, D. Deacu, J.-M. Bélanger, S. Skachko, Y. Liu, F. Dupont, J.-F. Lemieux, C. Beaudoin, B. Tranchant, M. Drévillon, G. Garric, C.-E. Testut, J.-M. Lellouche, P. Pellerin, H. Ritchie, Y. Lu, F. Davidson, M. Buehner, A. Caya, M. Lajoie, 2014: Sea ice forecast verification in the Canadian Global Ice Ocean Prediction System. Submitted to the Quarterly Journal of the Royal Meteorological Society.

Weiss, J., E. M. Schulson, and H. L. Stern, 2007: Sea ice rheology from in-situ, satellite and laboratory observations: Fracture and friction. Earth and Planetary Science Letters, 255, 1–8.

Weiss, J. and E.M. Schulson. 2009: Coulombic faulting from the grain scale to the geophysical scale: lessons from ice. Journal of Physics D, 42(21), 214017, doi:10.1088/0022-3727/42/21/214017.

Notebook

Editorial Board:

Laurence Crosnier and
Gilles Garric

DTP Operator:

BBS Studio

Articles:

Contact :
Please send us your comments to the following e-mail address: webmaster@mercator-ocean.fr